BIOCHEMISTRY
including biophysical chemistry & molecular biology

Article

pubs.acs.org/biochemistry

Structure and Dynamics of *Brachypodium* Primary Cell Wall Polysaccharides from Two-Dimensional ^{13}C Solid-State Nuclear Magnetic Resonance Spectroscopy

Tuo Wang,[†] Andre Salazar,[‡] Olga A. Zabotina,[‡] and Mei Hong*[,†]

[†]Department of Chemistry and Ames Laboratory and [‡]Department of Biochemistry, Biophysics and Molecular Biology, Iowa State University, Ames, Iowa 50011, United States

Supporting Information

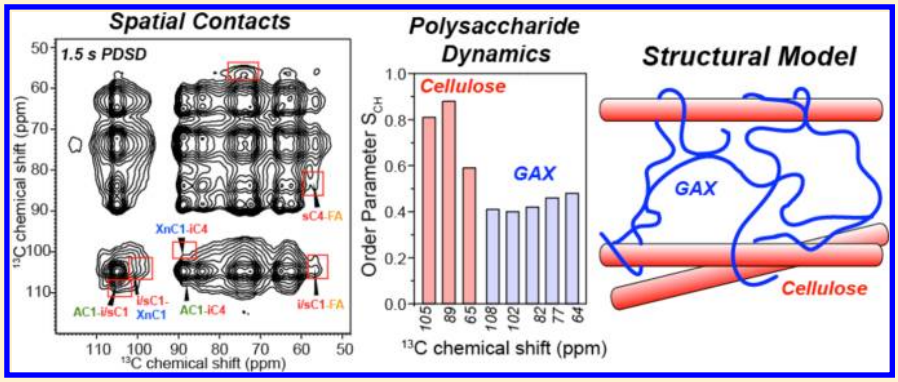

ABSTRACT: The polysaccharide structure and dynamics in the primary cell wall of the model grass *Brachypodium distachyon* are investigated for the first time using solid-state nuclear magnetic resonance (NMR). While both grass and non-grass cell walls contain cellulose as the main structural scaffold, the former contains xylan with arabinose and glucuronic acid substitutions as the main hemicellulose, with a small amount of xyloglucan (XyG) and pectins, while the latter contains XyG as the main hemicellulose and significant amounts of pectins. We labeled the *Brachypodium* cell wall with ^{13}C to allow two-dimensional (2D) ^{13}C correlation NMR experiments under magic-angle spinning. Well-resolved 2D spectra are obtained in which the ^{13}C signals of cellulose, glucuronoarabinoxylan (GAX), and other matrix polysaccharides can be assigned. The assigned ^{13}C chemical shifts indicate that there are a large number of arabinose and xylose linkages in the wall, and GAX is significantly branched at the developmental stage of 2 weeks. 2D $^{13}C-^{13}C$ correlation spectra measured with long spin diffusion mixing times indicate that the branched GAX approaches cellulose microfibrils on the nanometer scale, contrary to the conventional model in which only unbranched GAX can bind cellulose. The GAX chains are highly dynamic, with average order parameters of ∼0.4. Biexponential ^{13}C T_1 and ^{1}H $T_{1\rho}$ relaxation indicates that there are two dynamically distinct domains in GAX: the more rigid domain may be responsible for cross-linking cellulose microfibrils, while the more mobile domain may fill the interfibrillar space. This dynamic heterogeneity is more pronounced than that of the non-grass hemicellulose, XyG, suggesting that GAX adopts the mixed characteristics of XyG and pectins. Moderate differences in cellulose rigidity are observed between the *Brachypodium* and *Arabidopsis* cell walls, suggesting different effects of the matrix polysaccharides on cellulose. These data provide the first molecular-level structural information about the three-dimensional organization of the polysaccharides in the grass primary wall.

Grasses have long contributed to human society as cereal crops for human diets and forage for animals. Recently, growing interest has been directed toward developing grasses as a major source of alternative, renewable energy. The polysaccharides stored in grass cell walls (CWs) can be extracted and converted into biofuels;[1,2] thus, an understanding of the polysaccharide structures in the CWs is important for efficient degradation of this biomass.[3] *Brachypodium distachyon* has been adopted as a model plant for structural and functional genomics of grasses, because it has a short lifecycle and a small genome, is self-pollinating, and is representative of many temperate grasses.[4] Thus, a detailed understanding of the molecular structure and composition of the *Brachypodium* CWs in their native state is of significant interest.

The primary CW (PCW) of monocotyledonous (monocot) plants such as grasses differs from the PCW of dicotyledonous (dicot) plants as represented by *Arabidopsis thaliana*. In dicot PCWs, the main hemicellulose is xyloglucan (XyG), and the main pectins are linear homogalacturonan (HGA) and branched rhamnogalacturonan (RG), which contains arabinan, galactan (Gal), and arabinogalactan (AG) side chains.[5,6] In

Received: February 23, 2014
Revised: April 4, 2014
Published: April 10, 2014

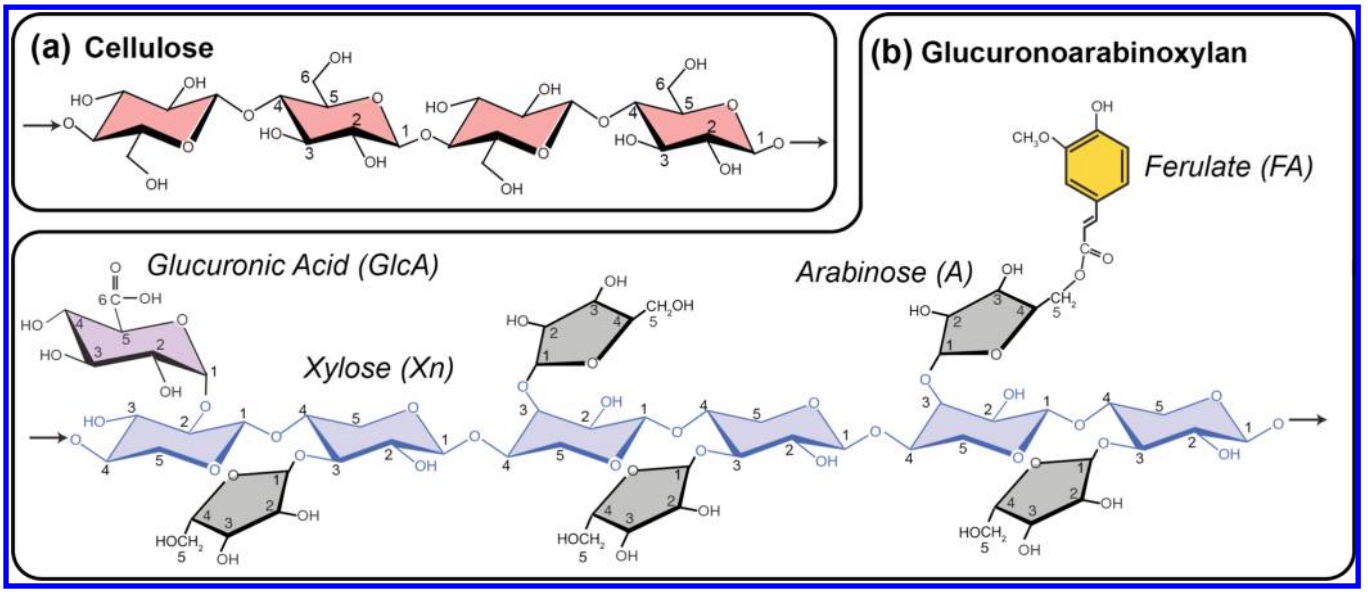

Figure 1. Chemical structures of major polysaccharides in the grass PCW: (a) cellulose and (b) glucuronoarabinoxylan.

grass PCWs, the main hemicelluloses are glucuronoarabinoxylans (GAX) and mixed-linkage glucan (MLG). GAX consists of a (1 → 4) β-linked xylose (Xyl) backbone substituted with arabinose (Ara) at the O3 position and glucuronic acid (GlcA) at the O2 position (Figure 1). Some of the Ara side chains are further esterified with ferulic acid (FA), which may cross-link multiple xylan (Xn) chains through dimerization.[7] MLG is a copolymer of (1 → 4) and (1 → 3) β-linked glucose and is enriched in the walls of elongating plant cells.[8] Grass PCWs also contain XyG, HGA, and RG, but their concentrations are much lower than in dicot PCWs.[9] The amount of structural proteins is also negligible in the grass PCW.[10]

While the composition of plant CWs can be obtained from chemical extractions followed by monosaccharide and linkage analysis, the three-dimensional structural arrangement of wall polysaccharides is more difficult to characterize because of the insoluble and amorphous nature of most of these polymers and the perturbing nature of chemical extraction. X-ray diffraction studies of plant CWs focused on the crystalline cellulose[11,12] and not the amorphous matrix polysaccharides. Electron and atomic force microscopy of plant CWs[13−15] lack the atomic resolution and chemical specificity. Solution nuclear magnetic resonance (NMR) studies require dissolution treatment of the CWs.[16,17] One-dimensional ^{13}C solid-state NMR has been used to study cellulose in various organisms[18−20] but cannot easily resolve the signals of different polysaccharides in an intact CW.

Recently, we introduced multidimensional magic-angle-spinning (MAS) solid-state NMR spectroscopy for studying the structure of plant CW polysaccharides. By ^{13}C labeling whole plants, we achieved the sensitivity necessary for two-dimensional (2D) and three-dimensional (3D) correlation NMR experiments, which in turn provide the resolution needed for understanding the structure and dynamics of multiple wall polysaccharides.[6,21,22] The first organism we studied using this approach is the PCW of *Arabidopsis thaliana*. The 2D and 3D SSNMR spectra indicate that cellulose, XyG, and pectins form a single noncovalent network in the dicot PCW: both XyG and pectins show direct through-space cross peaks with cellulose, indicating spatial contacts within a nanometer. However, the sparseness of XyG−cellulose cross peaks indicates that XyG does not coat the microfibril surface extensively but may instead be embedded at specific locations in the microfibril.[6,22] These results revise the prevailing model of PCWs, in which pectins and proteins are envisioned to form a network separate from the cellulose−hemicellulose network.[5] The dicot wall polysaccharides are heterogeneously mobile: pectins are the most dynamic, and cellulose is the most rigid; hemicellulose exhibits intermediate mobility.[21] A XyG-deficient *Arabidopsis* mutant exhibits enhanced mobilities for the remaining wall polysaccharides,[6] consistent with the cross-linking function of XyG. In comparison, a partially depectinated sample displays a much higher rigidity for the remaining polysaccharides.[21] Loosening of this single-polysaccharide network by the protein expansin was achieved by expansin binding to cellulose, as shown using a sensitivity-enhanced NMR technique called dynamic nuclear polarization.[23] Moreover, the expansin-binding site of cellulose is enriched in XyG, suggesting that the XyG-bound positions of cellulose may be mechanical hot spots for CW loosening.[24]

Compared to that of dicot PCWs, the three-dimensional structure of grass PCWs has not yet been studied using multidimensional SSNMR. The existing model of grass PCW architecture depicts GAX as taking the role of XyG to cross-link cellulose microfibrils.[5] The physical interactions between GAX and cellulose are believed to depend on GAX branching: linkage analyses[8,25] and FT-IR data of sequentially extracted grass cell walls[26] indicate that highly substituted GAX are extracted by dilute base, while less branched GAX and MLG require more concentrated base to be extracted.[5,9] Scanning electron microscopy data of GAX-extracted cell walls showed a reduced matrix content between cellulose microfibrils.[26] These results led to the proposal that highly substituted GAX forms the interstitial matrix between cellulose microfibrils, while less branched GAX hydrogen bonds with cellulose. However, *in vitro* binding assays indicate that none of the extracted GAX binds cellulose well: only 4−15% of GAX of any fraction binds to cellulose,[25] in contrast to the tight binding between XyG and cellulose.[27,28] Compared to GAX, MLGs are present at low concentrations in embryonal cell walls, but the concentrations increase significantly during growth.[25] Because current understanding of the grass PCWs comes from extraction-based chemical and ultrastructural analysis, high-resolution structural

dx.doi.org/10.1021/bi500231b | *Biochemistry* 2014, 53, 2840−2854

studies by SSNMR under nonperturbing conditions will provide valuable and unique information.

In this study, we report the first comprehensive assignment of the ^{13}C chemical shifts of *Brachypodium* primary wall polysaccharides and provide evidence of GAX−cellulose spatial contact in 2D $^{13}C-^{13}C$ correlation spectra. We also investigated the mobilities of wall polysaccharides and show that GAX has larger-amplitude motions than its counterpart, XyG, in the dicot PCW. These results shed light on the 3D architecture of the grass PCW and establish a basis for future studies of grass cell walls.

EXPERIMENTAL PROCEDURES

Plant Material. Uniformly ^{13}C-labeled *B. distachyon* PCW samples were prepared using a procedure similar to that reported previously.[6] Briefly, plants were germinated and grown in the dark in a liquid containing ^{13}C-labeled glucose (5 g/L) as the only carbon source. Growth in the dark prevents photosynthesis and the consequent dilution of ^{13}C labels by unlabeled substrates produced from atmospheric CO_2. Two-week-old seedlings were harvested, and roots and leaves were separated and powdered in liquid nitrogen, mixed with 80% (v/v) ethanol, heated at 80 °C for 1 h, and cooled to room temperature. PCWs were pelleted by centrifugation at 12000*g* for 20 min. The PCW material was never dried throughout the preparation. The wet pellet was washed with a chloroform/methanol (1:1) solution to remove nonpolar compounds and suspended in 50 mM sodium acetate buffer (pH 5.2) containing 1.5% SDS and 5 mM sodium metabisulfate to remove most intracellular proteins and low-molecular weight compounds. Starch was removed using α-amylase. These procedures are expected to have a minimal impact on the wall polysaccharides and structural proteins because of their low solubility and their interaction via hydrogen bonding or covalent cross-linking. Two samples were prepared from the roots and leaves of the plant. Approximately 76 mg of hydrated leaf CW and 58 mg of hydrated root CW were packed into two 4 mm MAS rotors for SSNMR experiments. A previously prepared ^{13}C-labeled *Arabidopsis* PCW sample[6] was used to compare with the *Brachypodium* PCW samples.

Solid-State NMR Spectroscopy. All ^{13}C NMR spectra were measured on a 600 MHz Avance II SSNMR spectrometer at 14.1 T using a 4 mm MAS probe. Typical radiofrequency (rf) field strengths were 62−71 kHz for ^{1}H and 50 kHz for ^{13}C. ^{13}C chemical shifts were externally referenced to the Met Cε peak (14.0 ppm) in the model peptide formyl-Met-Leu-Phe-OH[29,30] on the TMS scale.

One-dimensional (1D) ^{13}C MAS spectra were measured with either $^{1}H-^{13}C$ cross-polarization (CP) or ^{13}C direct polarization (DP) to create the initial transverse magnetization. CP spectra preferentially detect rigid molecules such as cellulose, while DP spectra with a short recycle delay (2 s) preferentially detect the signals of mobile polysaccharides. Quantitative spectra were measured using a DP experiment with a recycle delay of 15 s.

Several 2D $^{13}C-^{13}C$ correlation experiments were conducted to resolve and assign the ^{13}C chemical shifts of wall polysaccharides. The 2D J-INADEQUATE experiment[31,32] correlates the double-quantum (DQ) or sum chemical shifts of two directly bonded ^{13}C spins with the single-quantum (SQ) chemical shifts of each ^{13}C. The experiment used DP, $^{13}C-^{13}C$ *J* coupling, and a recycle delay of 2 s to preferentially detect the signals of mobile matrix polysaccharides. The experiment was conducted at 293 K under 12 kHz MAS. A double-quantum-filtered (DQF) 2D $^{13}C-^{13}C$ correlation spectrum complements the J-INADEQUATE experiment by detecting one-bond cross peaks of rigid polysaccharides. This experiment used SPC5-recoupled[33] $^{13}C-^{13}C$ dipolar coupling for polarization transfer and was conducted at 253 K under 7 kHz MAS. To probe intermolecular contacts, we measured 2D ^{1}H-driven ^{13}C spin diffusion (PDSD) spectra[22,34] with mixing times of 30 ms to 3.0 s. These PDSD experiments used either CP (at 253 K) or DP (at 293 K) to generate the initial ^{13}C magnetization. A PDSD experiment with a short CP contact time of 35 μs was conducted at 293 K to selectively detect only the cellulose signals in the indirect dimension, whose cross peaks with GAX in the direct dimension can thus be better resolved in the 2D spectra.

Motional amplitudes were measured using the dipolar-doubled 2D $^{13}C-^{1}H$ dipolar chemical shift (DIPSHIFT) correlation experiment[35,36] under 7 kHz MAS. ^{1}H homonuclear decoupling was achieved using the FSLG sequence,[37] which has a theoretical scaling factor of 0.577. The rigid-limit one-bond C−H dipolar coupling, after doubling and scaling, was found to be 26.2 kHz on the crystalline model peptide formyl-MLF-OH.[29,38] The ratios between the measured couplings of the polysaccharides and this rigid-limit value gave the order parameters.

^{13}C T_1 relaxation times, which reveal nanosecond motions, were measured using the inversion recovery sequence. The initial ^{13}C magnetization was excited using a single pulse, and a long recycle delay of 15 s was used to obtain quantitative spectra. ^{13}C-detected ^{1}H $T_{1\rho}$ relaxation times, which reflect microsecond motions, were measured using a Lee−Goldburg spin-lock sequence[39−41] in which ^{1}H spin diffusion was suppressed during the spin-lock period and the CP period to obtain site-specific relaxation times of the protons that are directly bonded to a ^{13}C spin. The tilted effective ^{1}H spin-lock field was 50 kHz. Most relaxation curves were fit with a double-exponential function (Tables S1 and S2 of the Supporting Information).

Monosaccharide Composition Analysis. Approximately 30 mg of PCWs from the *Brachypodium* leaves and roots was hydrolyzed in 2 M trifluoroacetic acid for 2 h at 121 °C, after which the acid was removed when the sample was dried under air at 50 °C. The dry material was solubilized in 100 μL of ddH_2O, and the monosaccharide composition was determined using high-performance anion-exchange chromatography.

The cellulose content was estimated by treating 10 mg of CW material with acetic−nitric reagent (80% acetic acid and concentrated nitric acid, 10:1) for 30 min at 100 °C.[24] Undigested pellets were washed several times with deionized water and then acetone, air-dried, and weighed.

Glycosyl Linkage Analysis. The PCW samples were permethylated, depolymerized, reduced, and acetylated. The resulting partially methylated alditol acetates (PMAAs) were analyzed by gas chromatography and mass spectrometry (GC−MS) as previously described.[42] Briefly, a 1−2 mg sample was suspended in DMSO, permethylated by the addition of Hakomori base while being purged with nitrogen gas, and mixed for 7 h. Iodomethane was then added, and the sample was mixed overnight. The sample then passed through a C18 SEP-PAK column, dried, and reduced with lithium borodeuteride in THF, which was neutralized and evaporated later. The sample was then treated with NaOH and methyl iodide in dry DMSO.[43] The sample was subjected to 4 M NaOH for 15 min;

methyl iodide was added, and the mixture was left for 40 min to ensure complete methylation. The permethylated material was hydrolyzed using 2 M TFA, reduced with $NaBD_4$, and acetylated using acetic anhydride and TFA. The resulting PMAAs were analyzed by GC−MS. Separation was performed on a 30 m Restek 2330 or Supelco 2380 bonded phase fused silica capillary column.

RESULTS

***Brachypodium* Cell Wall Composition from Linkage Analyses and Quantitative ^{13}C NMR.** We obtained ^{13}C-labeled *Brachypodium* PCW by growing the plant for 2 weeks in the dark with ^{13}C-labeled glucose as the only carbon source, harvesting the roots and leaves, and preparing the insoluble CW material as described previously[6] except without drying. This cell wall preparation procedure was mild, without involving strong acids or bases. Previous comparison of *Arabidopsis* PCW samples obtained from plants grown in light without extraction versus plants grown in the dark with mild treatment showed similar polysaccharide ^{13}C intensities,[22] even though the *Arabidopsis* PCW has more pectins, which can be extracted more easily.

At 2 weeks, the *Brachypodium* PCW is expected to contain mainly cellulose and GAX. Linkage analysis (Table 1) shows

Table 1. Glycosyl Linkage Composition of the *Brachypodium* Leaf Primary CW

glycosyl residue	peak area (%)
terminally linked arabinofuranosyl (t-Ara*f*)	13.5
4-linked arabinopyranosyl (4-Ara*p*) or 5-linked arabinofuranosyl (5-Ara*f*)	10.4
3-linked arabinofuranosyl residue (3-Ara*f*)	2.4
2-linked arabinofuranosyl (2-Ara*f*)	1.9
terminally linked arabinopyranosyl (t-Ara*p*)	0.3
4-linked glucopyranosyl (4-Glc*p*)	19.7
terminally linked glucopyranosyl (t-Glc*p*)	2.4
4,6-linked glucopyranosyl (4,6-Glc*p*)	0.6
3,4-linked glucopyranosyl (3,4-Glc*p*)	0.4
4-linked xylopyranosyl (4-Xyl*p*)	11.9
3,4-linked xylopyranosyl (3,4-Xyl*p*)	5.0
2,4-linked xylopyranosyl (2,4-Xyl*p*)	1.2
terminally linked xylopyranosyl (t-Xyl*p*)	0.8
terminally linked galactopyranosyl (t-Gal*p*)	6.5
4-linked galactopyranosyl (4-Gal*p*)	5.6
3-linked galactopyranosyl (3-Gal*p*)	1.1
6-linked galactopyranosyl (6-Gal*p*)	1.1
3,6-linked galactopyranosyl (3,6-Gal*p*)	0.4
2,4-linked rhamnopyranosyl (2,4-Rha*p*)	6.5
3,4-linked mannopyranosyl (3,4-Man*p*)	2.7
4-linked mannopyranosyl (4-Man*p*)	2.0
2,4-linked manopyranosyl (2,4-Man*p*)	0.5
4,6-linked galacturonopyranosyl acid (6-Gal*p*A)	2.1
6-linked glucuronopyranosyl acid (6-Glc*p*A)	1.2
total	100.0

that 4-Xyl, 2,4-Xyl, and 3,4-Xyl account for 19% of all linkages. Xyl O3 is 4 times more substituted than O2, indicating that Ara is predominantly linked to Xyl O3 in the grass PCW, and Ara dominates GlcA in the xylan side chains. The Xyl concentration from the linkage analysis is lower than that from the sugar composition analysis (Table 2). This discrepancy may result from the incomplete accessibility of GAX to methylation

Table 2. Monosaccharide Compositions (mole percentage) of the 4 M NaOH Soluble Fraction and Cellulose Contents (microgram per milligram of dry CW) in the *Brachypodium* Primary CW

residue	root	leaf
Fuc	0.2 ± 0.05	0.1 ± 0.0
Rha	0.9 ± 0.2	1.2 ± 0.2
Ara	14.9 ± 0.5	20.9 ± 0.8
Gal	11.1 ± 1.1	5.9 ± 0.2
Glc	17.8 ± 1.8	23.7 ± 1.5
Xyl	52.3 ± 2.3	44.7 ± 1.8
Man	1.3 ± 0.05	0.8 ± 0.1
GalA	0.1 ± 0.0	0.8 ± 0.05
GlcA	1.4 ± 0.05	1.9 ± 0.1
cellulose	305.1	285.4

because of its low solubility. A significant amount of Ara was detected: t-Ara and 5-Ara can be assigned mostly to GAX, while the low levels of 2-Ara and 3-Ara may be assigned to arabinan and arabinogalactan proteins (AGPs).[44−46] In addition to GAX, the grass PCW can also contain other hemicelluloses such as XyG, MLG, and glucomannan.[9] Sugar and linkage analyses showed that XyG was indeed present (4,6-Glc) but no MLG can be detected, because no 3-Glc linkage was found (Table 1). This is consistent with the fact that the level of MLG is known to vary greatly with developmental stage.[47,48] The common pectic sugars such as 2,4-Rha (6.5%), 4,6-GalA (2.1%), and 4-Gal (5.6%) occur at low concentrations, as expected.

Quantitative 1D ^{13}C MAS spectra of the *Brachypodium* leaf and root PCWs (Figure 2a) show identical ^{13}C chemical shifts and very similar intensity distributions, indicating that roots and leaves have similar polysaccharide compositions at 2 weeks of

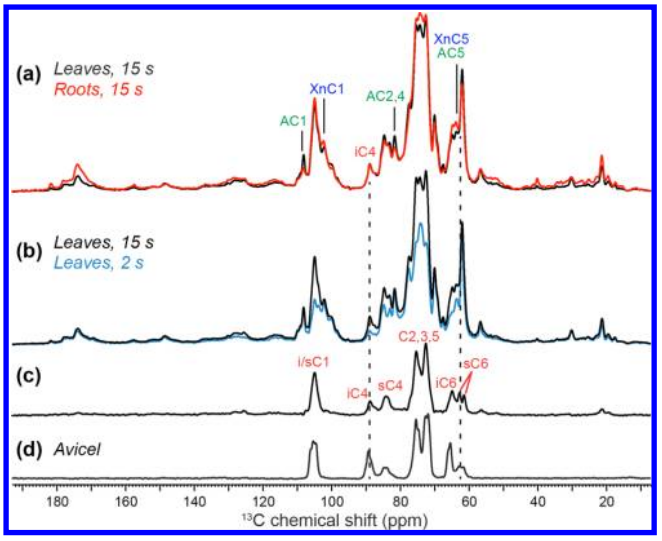

Figure 2. 1D ^{13}C MAS spectra of the uniformly ^{13}C-labeled *Brachypodium* primary cell wall. (a) Quantitative DP spectra of cell walls of leaves (black) and roots (red), measured with a 15 s recycle delay. (b) DP spectra of leaves with 2 s (blue) and 15 s (black) recycle delays. (c) Difference spectrum between the two DP spectra in part b. The peak positions match the cellulose chemical shifts, indicating that the main rigid polysaccharide in the *Brachypodium* PCW is cellulose. (d) ^{13}C CP-MAS spectrum of microcrystalline cellulose (Avicel Ph-101). The surface (s) amorphous cellulose signals are much weaker in Avicel than in spectrum c, consistent with the highly crystalline nature of Avicel.

dx.doi.org/10.1021/bi500231b | *Biochemistry* 2014, 53, 2840−2854

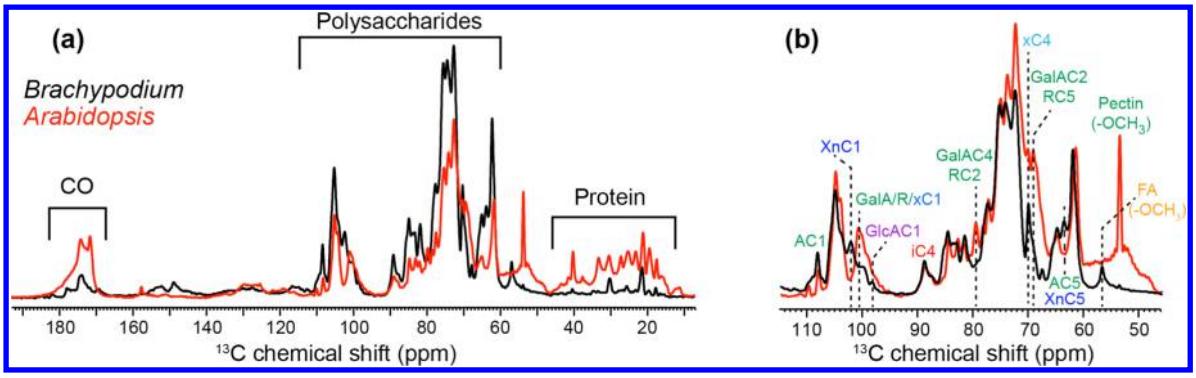

Figure 3. 1D ^{13}C quantitative MAS spectra of *Brachypodium* (black) and *Arabidopsis* (red) primary cell walls. (a) Spectra plotted with the same total integrated intensities. (b) Spectra plotted to have the same iC4 peak intensity at 89 ppm. The *Brachypodium* spectrum shows higher xylose (Xn), arabinose (A), and ferulic acid (FA) intensities and lower protein and pectin intensities. Representative pectin signals are the 101 ppm peak of galacturonic acid (GalA) and rhamnose (R) and the 53.5 ppm peak of methyl ester.

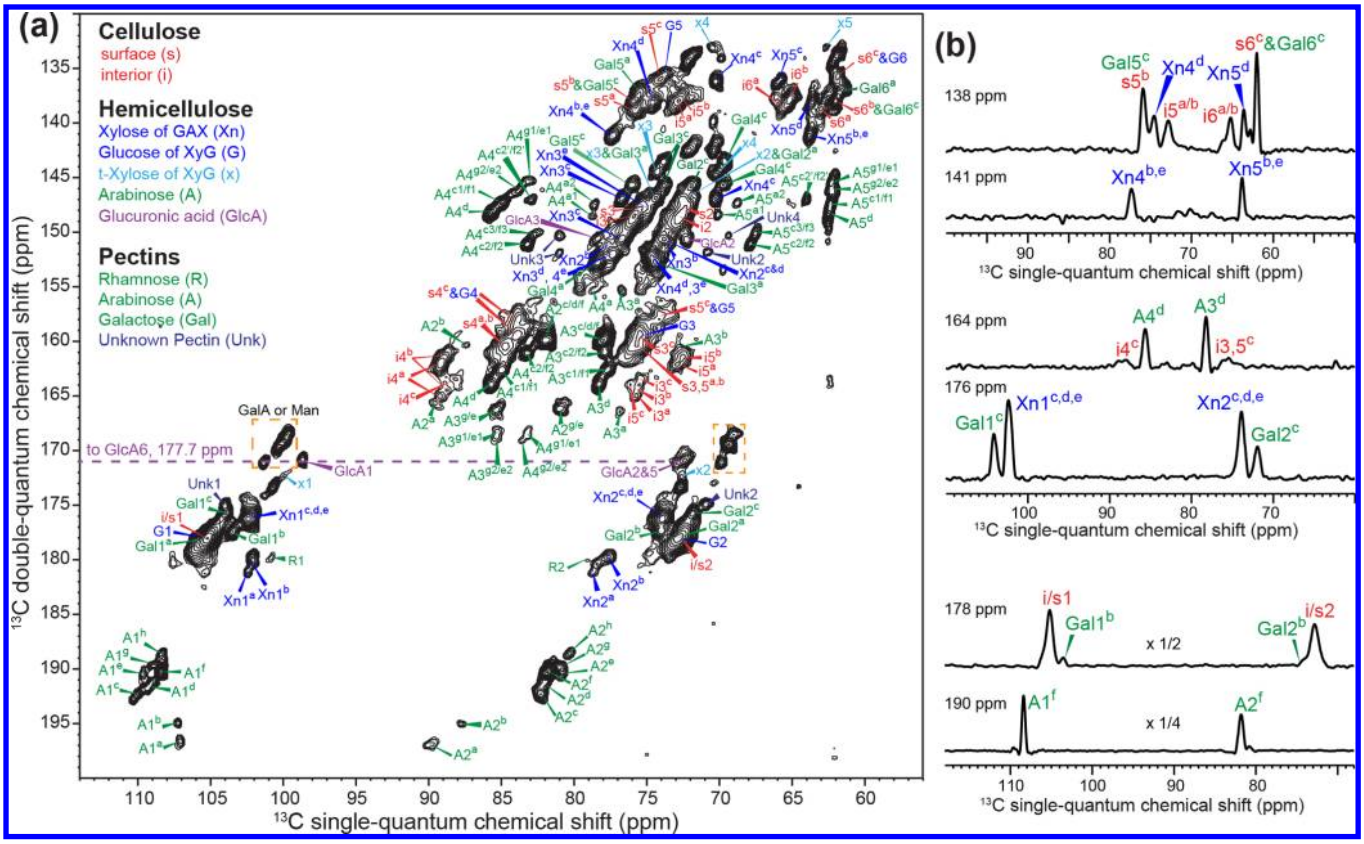

Figure 4. 2D ^{13}C J-INADEQUATE spectrum of the *Brachypodium* PCW, measured at 293 K under 12 kHz MAS. (a) Polysaccharide region of the 2D spectrum. (b) Selected 1D cross sections along the single-quantum (ω_2) dimension. Peaks are assigned using the abbreviations shown, and superscripts distinguish different subtypes of the same monosaccharide. For example, eight sets of arabinose C1−C2 cross peaks are identified and indicated by superscripts a−h.

age. Subtle differences in the relative intensities of Ara and Xn peaks are found between the two tissues: the leaf sample has slightly higher Ara intensities (108 ppm for AC1 and 82 ppm for AC2/C4) but lower Xn intensities (102 ppm for XnC1), indicating that the cell wall of leaves contains slightly more substituted GAX than the cell wall of leavess. The ^{13}C CP spectra (Figure S1 of the Supporting Information) are also very similar between the two samples, indicating that the polysaccharides have similar mobilities in the two tissues. When 1D ^{13}C DP spectra were measured using a short recycle delay to preferentially detect the mobile polysaccharides, the spectrum differed from the quantitative 1D spectrum by precisely the chemical shifts of crystalline and amorphous cellulose (Figure 2b,c),[18] as verified by comparison with the ^{13}C spectrum of Avicel cellulose (Figure 2d). However, the grass PCW spectrum has much higher intensities of the surface amorphous cellulose than the Avicel spectrum, consistent with the microcrystalline nature of Avicel. Overall, the main rigid polysaccharide in the *Brachypodium* PCW is cellulose, while hemicelluloses and pectins are mobile.

To investigate how the PCW compositions differ between *Brachypodium* and *Arabidopsis*, we compared the quantitative 1D ^{13}C spectra of the two plants (Figure 3). The *Brachypodium* sample shows protein (10−50 and 170−180 ppm) and pectin

dx.doi.org/10.1021/bi500231b | *Biochemistry* 2014, 53, 2840−2854

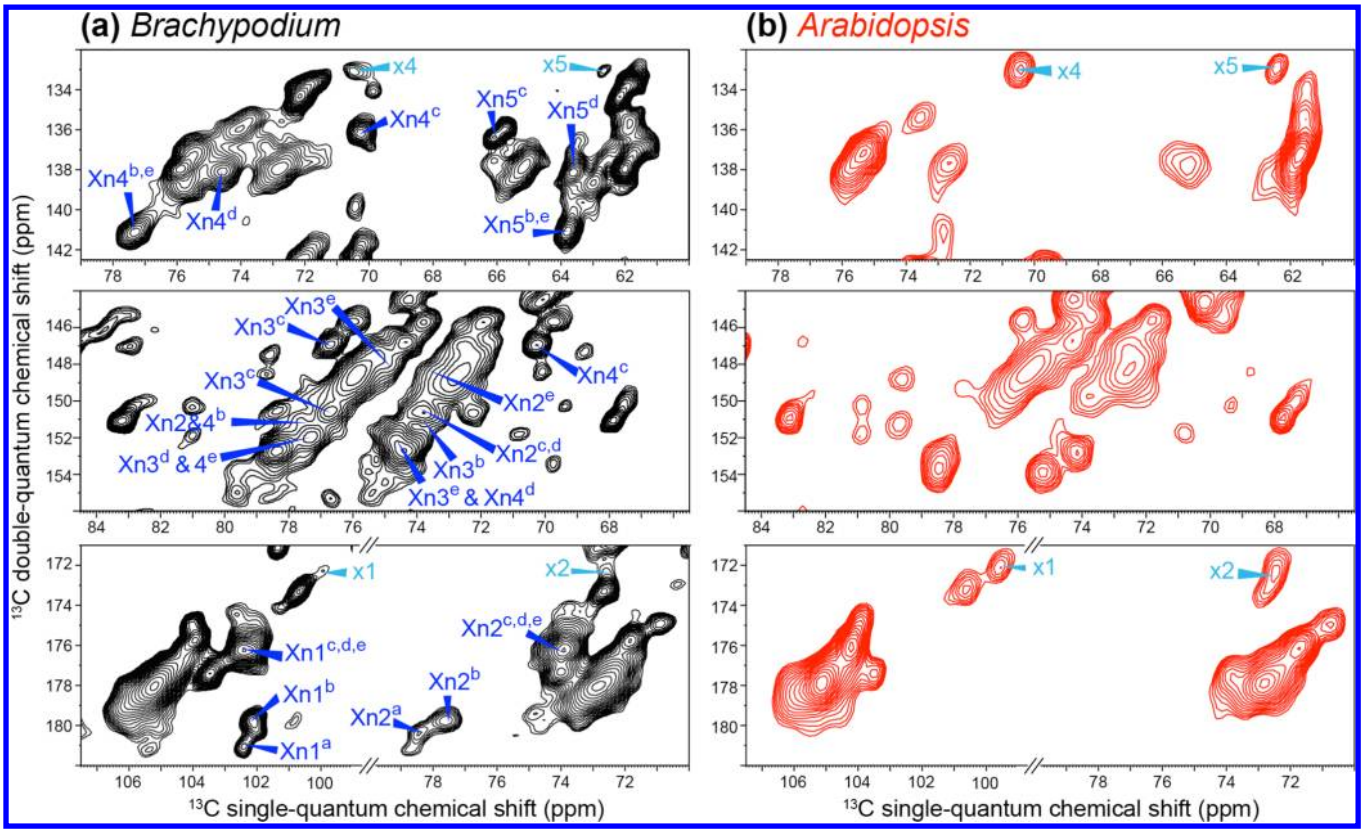

Figure 5. Assignment of hemicelluloses from the 2D J-INADEQUATE spectra of (a) *Brachypodium* and (b) *Arabidopsis* PCWs. *Brachypodium* shows numerous β-D-Xyl (Xn) signals and few α-D-Xyl (x) signals from XyG.

intensities lower than those of the *Arabidopsis* sample, both relative to the total spectral intensities and relative to the 89 ppm iC4 peak. For example, the 101 ppm peak of GalA and Rha C1 and the 80 ppm peak of GalA C4 and Rha C2 are weaker in the *Brachypodium* spectrum. The 53.5 ppm pectin methyl ester peak in the *Arabidopsis* spectrum is replaced by a 56 ppm ferulic acid (FA) methyl ester peak in the *Brachypodium* spectrum. However, the *Brachypodium* PCW has stronger Ara C1 (108 ppm) and Xn C1 (102 ppm) peaks, consistent with the fact that GAX primarily exists in grass.

^{13}C Resonance Assignments of *Brachypodium* Cell Wall Polysaccharides by 2D Correlation NMR. To fully resolve the signals of all polysaccharides, we measured a 2D J-INADEQUATE spectrum[31,49] at ambient temperature under conditions that favor the observation of the signals of mobile polysaccharides while disfavoring cellulose.[18] The resulting 2D spectrum (Figure 4) shows narrow line widths of 0.4−0.9 ppm, indicating the highly dynamic nature of the matrix polysaccharides. Several regions of the 2D spectrum are of particular interest. First, the regions with DQ chemical shifts of 132−156 and 172−182 ppm contain the Xyl peaks and are more crowded than the corresponding region of the *Arabidopsis* spectrum (Figure 5) because of the presence of both GAX and XyG in the grass PCW. Five different sets of Xn peaks are identified and denoted a−e. Types a and b are characterized by a C2 chemical shift of 77−78 ppm, which can be assigned to GlcA O2-substituted Xyl. This assignment is supported by the fact that the Xn^{a} and Xn^{b} peaks have intensities similar to those of the GlcA peaks (Figure 4a). Type c was assigned to terminal Xyl based on the C4 chemical shift of 70 ppm. We assigned Xn^{d} to Ara O2-substituted Xyl and Xn^{e} to unbranched xylan based on literature chemical shifts.[50,51] These Xn peaks are absent in the *Arabidopsis* spectrum.[10] In comparison, terminal Xyl signals that originate from XyG are stronger in the *Arabidopsis* spectrum. These α-Xyl signals of XyG differ from the β-Xyl signals of GAX because of the different configurations of the anomeric carbon.

Eight sets of Ara C1−C2 cross peaks (denoted a−h) are resolved in the 2D J-INADEQUATE spectrum based on the characteristic Ara C1 chemical shifts of 107−110 ppm[21,52] (Figure 6), while nine sets of Ara C4−C5 cross peaks can be resolved. Unfortunately, the C2−C3 and C3−C4 cross peaks of Ara partially overlap (Figure 6b) and cannot be assigned unambiguously. The successive levels of ambiguity in the C2−C3 and C3−C4 assignments are denoted by symbols such as A2$^{c/d/f}$ and A3$^{c2/f2}$, respectively. For example, while the C2 chemical shifts of Ara-c, -d, and -f are resolved in the C1−C2 region, they become overlapped in the C2−C3 region, giving rise to ambiguous A2$^{c/d/f}$ and A3$^{c/d/f}$ peaks. Subsequently, the Ara-c and Ara-f C3−C4 peaks acquire another 2-fold assignment ambiguity, as denoted by symbols such as A3$^{c1/f1}$ and A3$^{c2/f2}$. In the C4−C5 region, the A4$^{c2/f2}$ chemical shift further splits into A4$^{c2/f2}$ and A4$^{c2'/f2'}$. These assignment ambiguities create 17 possible combinations of Ara spin systems (Table 3), but only nine different Ara structures should exist in the sample, because only nine sets of C4−C5 cross peaks are resolved in the 2D spectrum. The Ara structural diversity in the grass PCW is understandable, because Ara exists not only in GAX side chains[9] but also in pectins and AGPs. The GAX side chain Ara can be substituted with FA, while the pectic arabinans can have linkages at O5, O2, and O3.[9,53] Finally, while the protein concentration in the grass CW is low, AGPs are ~90%

dx.doi.org/10.1021/bi500231b | *Biochemistry* 2014, 53, 2840−2854

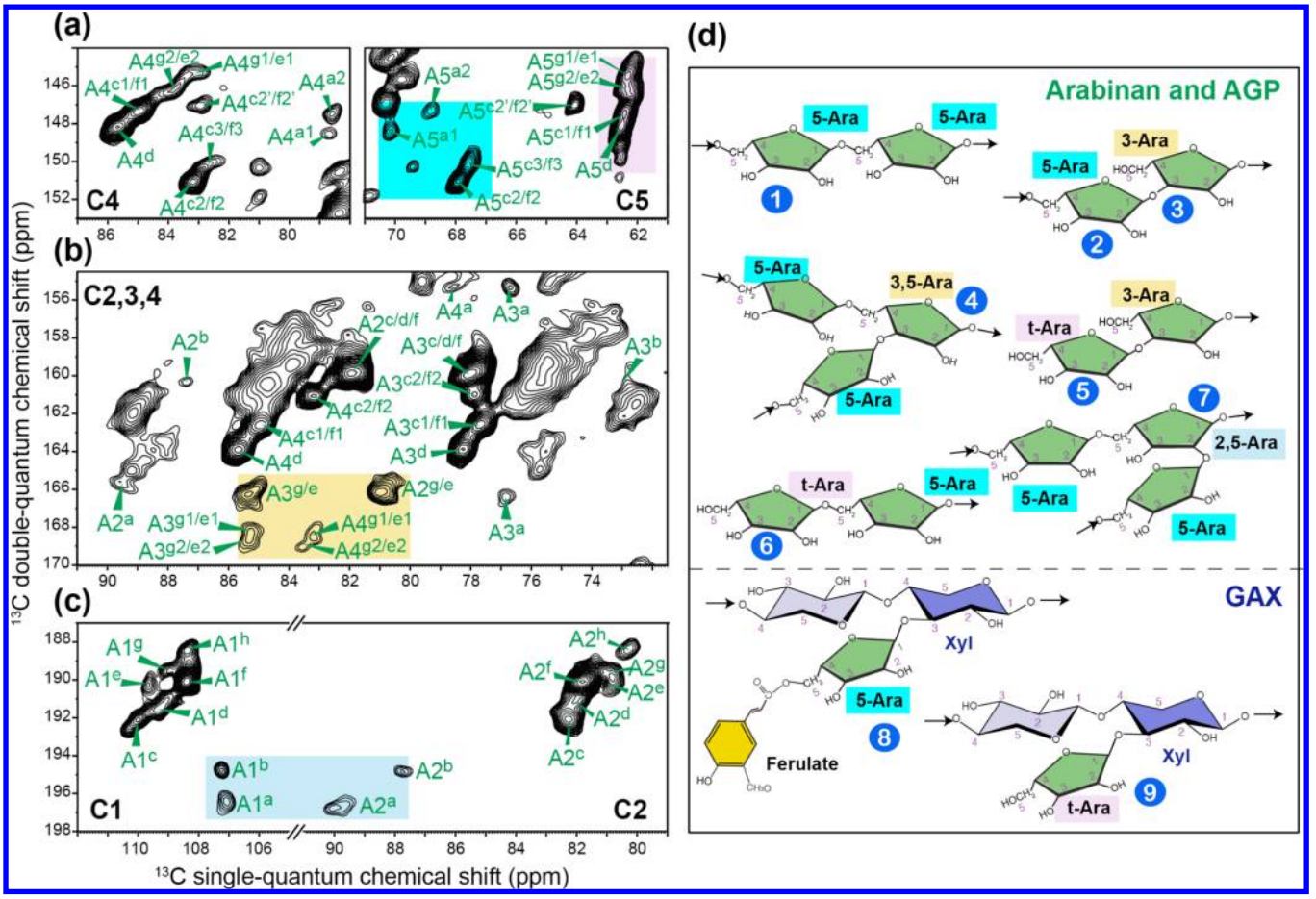

Figure 6. Assignment of arabinose signals and structures in *Brachypodium* PCW from the 2D J-INADEQUATE spectrum. (a) C4−C5 region of the 2D spectrum. (b) C2, C3, C4 region of the 2D spectrum. (c) C1−C2 region of the 2D spectrum. Spectral areas of t-Ara (pink), 5-Ara (cyan), 3-Ara (yellow), and 2-Ara (light blue) are shaded. Superscripts track the divergence and convergence of cross peaks. For example, $A3^{c/d/f}$ means the C3 peak of arabinose c, d, and f cannot be resolved. (d) Chemical structures of nine possible arabinose linkages that can occur in GAX, pectins, and AGPs.

carbohydrate and thus can still contribute significant intensities in the spectra.[45,46]

Figure 6d shows nine possible Ara linkages,[54] many of which can be matched to the spin systems in the 2D spectra. For example, Ara-a can be assigned to 2,5-Ara (structure 7) because its downfield C2 and C5 chemical shifts of 88−90 and 69−71 ppm indicate O2 and O5 substitutions, respectively. Similarly, Ara-b can be assigned to 2-Ara. Both Ara-a and Ara-b peaks are relatively weak, consistent with the linkage analysis that reveals that the 2-Ara concentration is low. Ara-e and Ara-g have downfield C3 chemical shifts of 85 ppm, indicating O3 substitution such as in structure 3 or 4. Ara-d, -c1, and -f1 have upfield C5 chemical shifts of ∼62 ppm, indicating that they are t-Ara. Among these three types, Ara-d has high intensities; thus, it is likely the common t-Ara in the GAX side chain (structure 9). This is also consistent with the fact that Ara-d C3−C4 cross peaks are absent in the *Arabidopsis* PCW (Figure S2 of the Supporting Information), which does not contain GAX. Ara types c2, f2, c3, and f3 can be assigned to 5-Ara because of their downfield C5 chemical shift of 64−68 ppm.

In addition to the polysaccharide region, the 2D INADEQUATE spectrum also shows two pairs of carboxyl−methyl cross peaks (Figure S3 of the Supporting Information). These can be assigned to the acetyl groups of O2- and O3-acetylated xylan,[55] because the other known acetylated polysaccharides, pectins and XyG, are present at very low levels in the *Brachypodium* PCW. The presence of O-acetylated GAX in the 2-week-old cell wall is interesting because O-acetylation is known to inhibit enzymatic degradation of wall polymers.[56]

Panels a and b of Figure 7 show the aromatic region of the 30 ms 2D PDSD spectrum, which exhibits multiple FA signals,[9,54] assigned from the unique FA methyl ester peak at 56 ppm. These measured FA ^{13}C chemical shifts do not give strong evidence of the presence of diferulic acid, which is expected to exhibit more downfield chemical shifts for the quaternary carbons. Interestingly, the FA cross peaks have asymmetric intensities with respect to the diagonal, with the top left peaks having much higher intensities than the bottom right peaks. This can be attributed to the different ^{1}H densities in the phenylene ring: the ^{1}H-bonded carbons such as C2 and C8 resonate in the top left half of the spectrum, whereas quaternary and carbonyl carbons resonate in the bottom right. A clear FA−Ara cross peak at (148, 108) ppm is observed, confirming the position of FA in the GAX side chain.

GlcA is present as a minor substituent at position O2 of the xylan backbone. We observed a carbonyl cross peak at (72.6, 177.5) ppm, which can be assigned to GlcA C5/2−C6 correlation (Figure 7c). The GlcA signals of the grass PCW are also observed in the 2D INADEQUATE spectrum. These

dx.doi.org/10.1021/bi500231b | *Biochemistry* 2014, 53, 2840−2854

Table 3. Assigned ^{13}C Chemical Shifts of *Brachypodium* Primary CW Polysaccharides from 2D J-INADEQUATE Spectra[a]

site	assignment	C1	C2	C3	C4	C5	C6	notes
i^a		105.0	72.9	75.8	89.2	72.9	65.2	
i^b		105.0	72.5	75.6	88.8	72.5	65.1	
i^c (w)		105.0	72.5	75.4	88.1	76.0	ND	
s^a		105.0	72.5	75.6	84.7	75.7	62.9	
s^b		105.0	72.5	75.6	84.7	75.9	62.0	
s^c		105.0	72.5	75.5	83.9	74.0	61.8	overlap with Glc of XyG
GlcA (w)	GlcA in GAX	98.6	72.4	78.3	ND	72.6	177.5	
Xn^a (w)	2,4-Xyl with GlcA attached to O2	102.4	78.6	ND	ND	ND		These peaks are absent in *Arabidopsis* CW.
Xn^b (w)		102.2	77.6	73.7	77.4	63.8		C3 chemical shift from Vignon et al.[64]
Xn^c	t-Xyl of GAX	102.4	73.9	*76.7*	70.2	66.0		These peaks are absent in *Arabidopsis* CW. Consistent with Hollmann et al.[50]
Xn^d	3,4-Xyl with Ara O3	102.4	73.9	76.7	74.6	63.6		These peaks are absent in *Arabidopsis* CW. Consistent with Roubroeks et al.[57]
Xn^e	4-Xyl of GAX	*102.4*	*73.7*	*75.0*	*77.4*	*63.8*		These peaks overlap with other Xn peaks and were obtained from Roubroeks et al.[57]
x	t-Xyl of XyG	99.6	72.5	74.2	70.4	62.6		α-Xyl C1 differs from β-Xyl in GAX by 2−3 ppm.
A^{a1} (w)	2,5-Ara	107.1	**89.8**	76.8	78.6	**70.7**		
A^{a2} (w)						**68.8**		
A^b (w)		107.3	**87.8**	72.6	ND	ND		
A^d	t-Ara of GAX	109.2	82.1	78.2	85.7	62.4		These peaks are absent in *Arabidopsis* CW.
A^{c1}	t-Ara	110.0	82.2	77.7	84.9	62.3		Consistent with Dick-Perez et al.[6]
A^{f1}		108.4	81.7					
A^{c2}	5-Ara	110.0	82.2	77.8	83.2	**67.9**		C5 chemical shifts consistent with Tan et al.[52]
A^{f2}		108.4	81.7					
$A^{c2'}$	5-Ara	110.0	82.2	77.8	83.0	**64.0**		
$A^{f2'}$		108.4	81.7					
A^{f3} (w)	5-Ara	108.4	81.7	77.8	82.5	**67.5**		
A^{c3} (w)		110.0	82.2					
A^{e1} (w)	3,5-Ara	109.6	80.8	**85.3**	83.3	62.3		C3 chemical shifts consistent with Hromadkova et al.[68] and Tan et al.[52]
A^{e2} (w)					83.6			
A^{g1} (w)		108.9	80.8	**85.3**	83.3	62.3		
A^{g2} (w)					83.6			
A^h		108.4	80.2	ND	ND	ND		
R (w)		100.8	79.1	ND	ND	69.2	17.8	C5−C6 peaks from the 30 ms PDSD spectrum
Gal^a		*105.0*	*72.5*	74.4	78.4	75.3	61.7	from Dick-Perez et al.[6]
Gal^b		103.4	74.0	*76.4*	*73.8*	*74.8*	*61.7*	from t-Gal (L) of Dick-Perez et al.[6]
Gal^c		103.9	71.9	73.8	69.5	75.8	61.8	present in both *Arabidopsis* and *Brachypodium* CWs
Unk (w)	unknown pectin	104.0	70.9	81.0	69.3	ND		present in WT and XG mutant *Arabidopsis* CW.[6] Lower intensities in depectinated CW.[21]
GalA/Man		100.2	69.3		ND			C1 and C2 shifts consistent with Dick-Perez et al.[6] and Jarvis et al.[69]
		99.6	69.0					
		101.3	69.8					

[a]The downfield chemical shifts that reflect the linkages of arabinoses are shown in bold. Unless specifically noted, most assignments are *de novo* based on the connectivity patterns in the 2D spectra. Weak signals are denoted (w). ND means not determined. Tentatively assigned ^{13}C chemical shifts are italicized and underlined.

GlcA peaks are readily distinguished from the 171 and 175 ppm GalA C6 peaks of the *Arabidopsis* PCW, which result from $COOCH_3$ and COOH.[22] The lack of these GalA signals in the *Brachypodium* sample is consistent with the absence of the 53.5 ppm methyl ester peak and indicates the low abundance of pectins in the grass PCWs.

In addition to GAX, the 2D J-INADEQUATE spectrum also resolved six different cellulose spin systems (Figure S4 of the Supporting Information). Cellulose is more rigid than GAX, as shown by the fact that its intensities are higher than those of the Xn, GlcA, and Ara signals in the 2D ^{13}C DQF correlation spectrum (Figure S5 of the Supporting Information). Compared to the *Brachypodium* spectrum, the *Arabidopsis* 2D DQF spectrum has much lower Ara and Xn intensities, consistent with a lack of GAX in the dicot PCW. On the other hand, the Gal C1−C2 cross peak at (101, 69) ppm is weaker in the *Brachypodium* spectrum, confirming that pectin concentrations are lower in the grass PCW.

None of these 2D spectra showed any signal near (86, 69) ppm, which are the expected frequencies of the C3−C4 cross peak for 3-Glc.[51,57−59] Thus, MLG is below the detection limit in the 2-week-old grass PCW.

GAX−Cellulose Intermolecular Contact from 2D ^{13}C PDSD Spectra. To determine if cellulose and GAX have spatial contact on the nanometer scale, we measured 2D $^{13}C-^{13}C$ PDSD spectra with mixing times from 30 ms to 3.0 s (Figure 8 and Figure S5 of the Supporting Information). At 30 ms, intraresidue cross peaks such as the Xn C1 correlations at 102 ppm and the Ara C1 correlations at 108 ppm are observed. When the mixing time increased to 1.5 s, multiple

dx.doi.org/10.1021/bi500231b | *Biochemistry* 2014, 53, 2840−2854

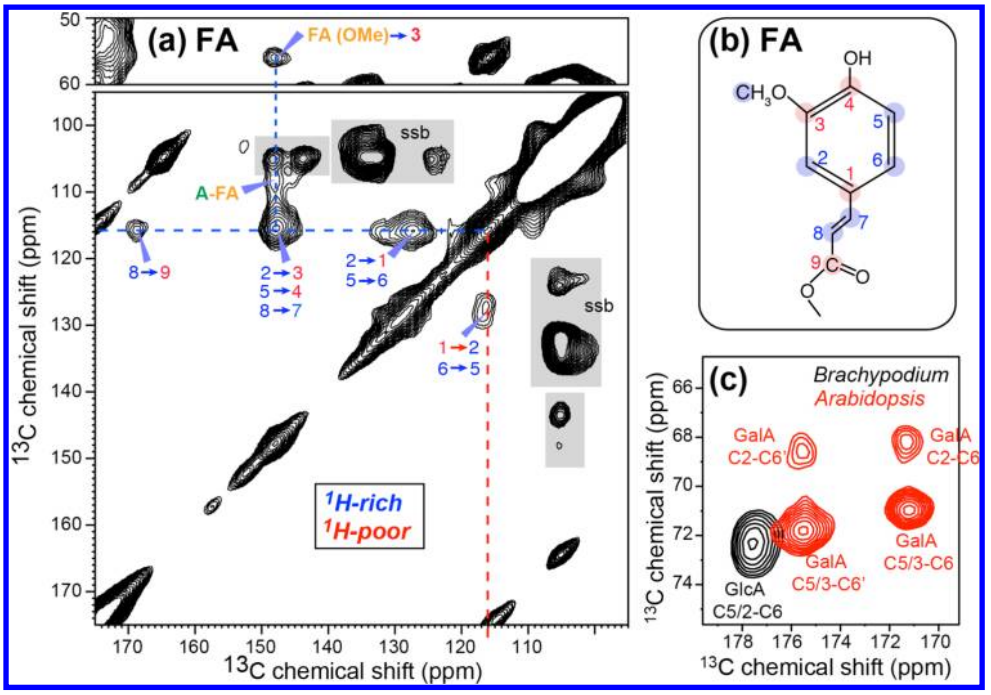

Figure 7. Assignment of GAX side chain signals from a 2D ^{13}C PDSD correlation spectrum measured at 253 K with a mixing time of 30 ms. (a) Aromatic region showing numerous FA signals. The ^{1}H-rich and ^{1}H-poor carbons are annotated in blue and red, respectively. Assignments are partly based on literature chemical shifts.[65] (b) Chemical structure of FA. (c) Assignment of a GlcA peak in the *Brachypodium* PCW (black) and GalA signals in the *Arabidopsis* PCW (red).

intermolecular GAX−cellulose cross peaks were detected, for example, between XnC1 and iC4 at (102, 89) ppm, between AC1 and iC4 at (108, 89) ppm, and between FA and cellulose at (89, 56) ppm. Thus, both GAX backbone and side chains are in molecular contact with the cellulose microfibrils. The 1D cross sections illustrate some of these cellulose−GAX cross peaks more clearly (Figure 8c).

To further verify the cellulose−GAX interactions, we measured an edited 2D correlation spectrum in which the cellulose signals are selectively detected in the indirect dimension by using a short CP contact time while all polysaccharides' signals are detected in the direct dimension after a mixing time. The resulting 2D spectra (Figure 9) show unambiguous cellulose−Xn and cellulose−Ara cross peaks after samples have been mixed for 3.0 s. However, these intermolecular cross peaks are weak, indicating that only a small fraction of cellulose is in close contact with GAX. Indeed, the cellulose cross sections have intensity patterns quite different from the GAX cross sections after samples have been mixed for 1.5 s (Figure 8c), indicating that the two polysaccharides are not homogeneously mixed on the 1 nm scale that is relevant for ^{13}C spin diffusion. This is not surprising, because the 3−5 nm diameter of the cellulose microfibril presents a significant spin diffusion barrier to the surrounding matrix polysaccharides.[22] In comparison, all GAX cross sections have similar intensity patterns, indicating that ^{13}C magnetization is equilibrated between the xylan backbone and the Ara and FA side chains.

Polysaccharide Mobilities in the *Brachypodium* Primary Cell Wall. To investigate polysaccharide mobilities in the *Brachypodium* PCW, we measured $^{13}C-^{1}H$ bond order parameters (S_{CH}) and ^{13}C T_1 and ^{1}H $T_{1\rho}$ relaxation times. Order parameters provide information about the motional amplitudes, while relaxation times reflect motional rates. The C−H order parameters were measured using the 2D DIPSHIFT experiment,[35] which yields time-dependent intensity decays indicative of the dipolar coupling strength. The matrix polysaccharides and cellulose show different dipolar decay rates, which allow their signals to be better resolved at chosen dipolar dephasing times. For example, with 41 μs dipolar dephasing, the 105 ppm peak of cellulose and Gal C1 was completely suppressed while the Ara (108 ppm) and Xn (102 ppm) C1 signals remain (Figure 10a). In the time domain dipolar cross sections (Figure 10b), cellulose exhibits much deeper intensity decays than GAX, indicating stronger dipolar couplings or higher order parameters. The cellulose S_{CH} values are 0.7−0.9, similar to the values of the *Arabidopsis* PCW sample (Figure 10c), and correspond to root-mean-square (rms) amplitudes of 15−26°.[40] GAX exhibits much smaller S_{CH} values of ∼0.4, indicating larger motional amplitudes. Interestingly, the GAX order parameters are noticeably smaller than the XyG order parameters in the *Arabidopsis* PCW and also smaller than the pectin S_{CH} values, indicating that GAX in the grass PCW is more mobile than most matrix polysaccharides in the dicot PCW.

The ^{13}C T_1 and ^{1}H $T_{1\rho}$ relaxation times are shown in Figure 11. Most ^{13}C sites exhibit double-exponential T_1 decays (Figure S6 of the Supporting Information), with a short T_1 component and a long T_1 component of <0.5 and >3 s, respectively. The long T_1 component is longer for cellulose (4−5 s) than for GAX (2−4 s). In addition, GAX contains a higher population of the faster-relaxing component while cellulose is dominated by the long T_1 component. These results are consistent with the order parameter data in indicating that GAX is much more mobile than cellulose on the nanosecond time scale. Because ^{13}C T_1 data contain spin diffusion effects, to obtain more site-specific relaxation times and to probe motion on a slower time scale, we measured the ^{1}H $T_{1\rho}$ values using a Lee−Goldburg

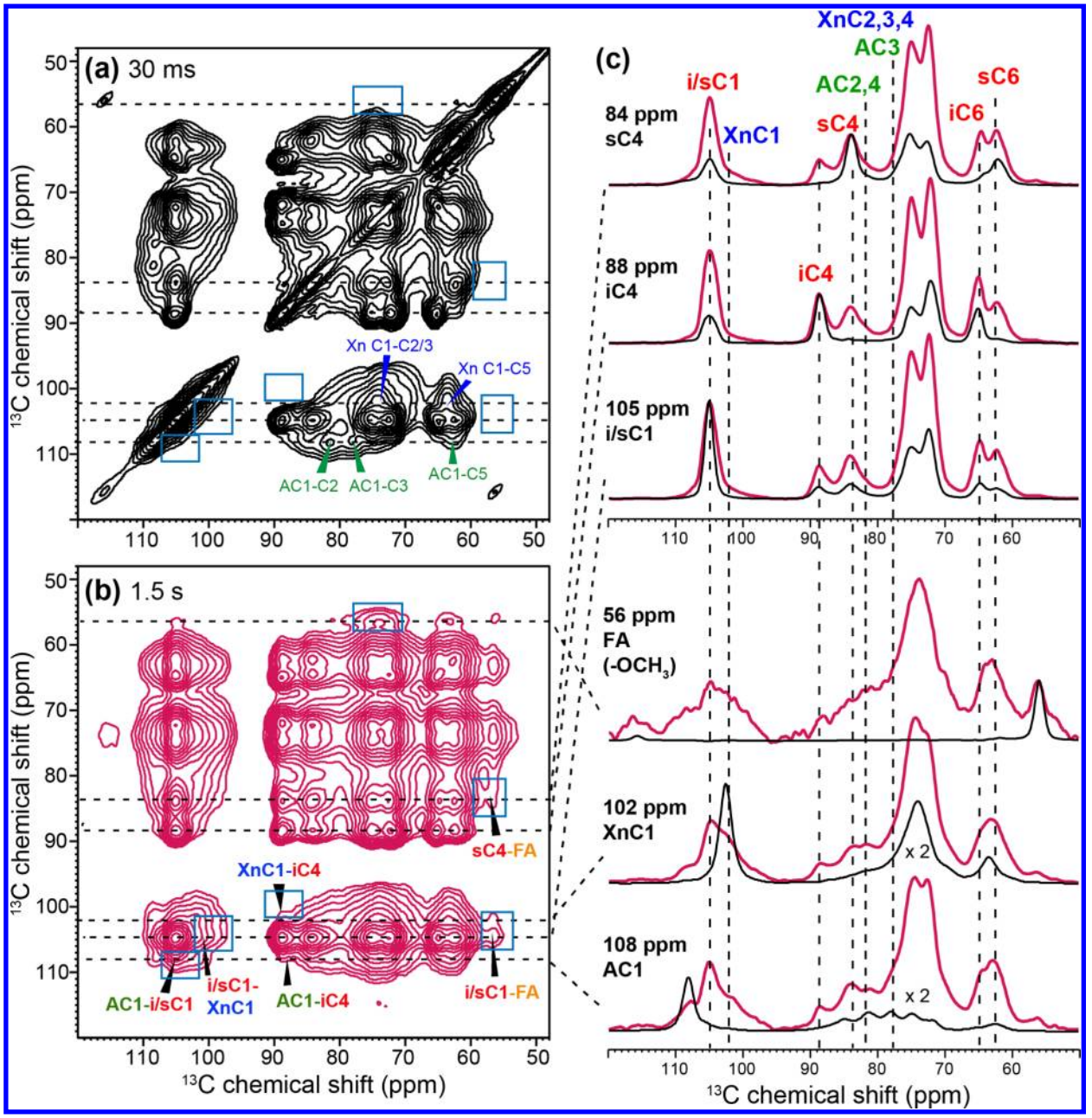

Figure 8. 2D ^{13}C PDSD spectra of the *Brachypodium* PCW with mixing times of (a) 30 ms and (b) 1.5 s. The spectra were measured at 253 K. (c) 1D cross sections from the 30 ms (red) and 1.5 s (black) 2D spectra. Several cellulose cross peaks to Xn, Ara, and FA in GAX cross peaks are observed by 1.5 s.

spin-lock experiment.[6,40] Similar to the ^{13}C T_1 data, GAX exhibits much shorter ^{1}H $T_{1\rho}$ values than cellulose, indicating faster motions. The short and long $T_{1\rho}$ components are similarly populated in GAX, while the long T_1 component dominates (~80%) in cellulose. Taken together, these data indicate that GAX undergoes faster motion than cellulose on both the nanosecond and microsecond time scales.

Comparing the *Brachypodium* and *Arabidopsis* samples, we find the relaxation times of GAX and XyG are similar but the fractions of the dynamic components are higher in GAX than in XyG. Cellulose in the two cell walls exhibits subtle differences: the slow-relaxing components in *Brachypodium* have longer relaxation times than in *Arabidopsis*. This result, together with the larger amplitude dynamics of GAX, suggests that cellulose–GAX interactions in the grass PCW are weaker than the cellulose–XyG interactions in the dicot PCW.

■ DISCUSSION

Brachypodium has recently been proposed as a model plant for grasses,[10] but structural characterization of the *Brachypodium* PCW has been scarce.[60] The study presented here establishes benchmark polysaccharide ^{13}C chemical shifts for the PCW of this model grass. The samples analyzed here are never dried; thus, the polysaccharide interactions and mobilities closely resemble those under the native condition. At 2 weeks of age, the roots and leaves have very similar quantitative ^{13}C spectra, indicating similar compositions of the CWs. Monosaccharide composition and linkage analyses (Tables 1 and 2) and ^{13}C SSNMR spectra indicate that the *Brachypodium* PCW mainly

dx.doi.org/10.1021/bi500231b | *Biochemistry* 2014, 53, 2840–2854

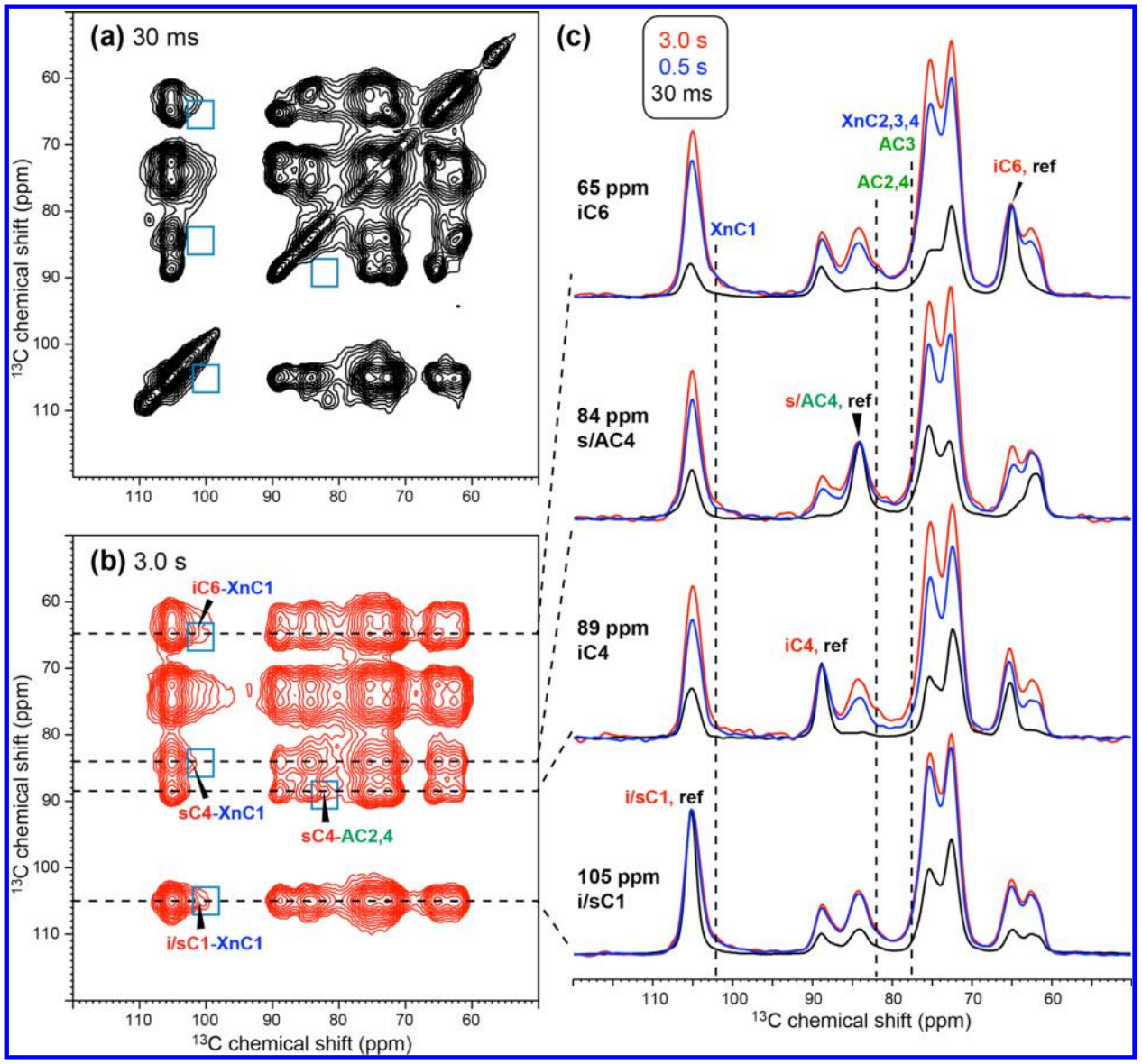

Figure 9. 2D ^{13}C PDSD correlation spectra of the *Brachypodium* PCW. The spectra were measured with a short CP contact time of 35 μs at 293 K to select cellulose signals in the indirect dimension and detect their cross peaks with matrix polysaccharides in the direct dimension. Mixing times are (a) 30 ms and (b) 3.0 s. (c) Representative cellulose cross sections as a function of mixing time, where increasing GAX intensities are observed.

consists of cellulose and GAX, followed by minor amounts of XyG and pectins. No MLG is found at this stage, which is consistent with endoglucanase assays that showed that the MLG concentration in *Brachypodium* peaked 2−3 days after germination and decreased to undetectable levels by day 8.[61] The minor amount of Glc found in these samples likely results from amorphous cellulose and XyG that are hydrolyzed under the conditions of monosaccharide analysis. Compared to the *Arabidopsis* PCW spectra, the *Brachypodium* spectra show larger amounts of xylan and smaller amounts of XyG and pectins.[9,10]

The high-resolution 2D ^{13}C correlation spectra of the never-dried grass PCW sample resolved nine Ara spin systems, five Xn spin systems, and six cellulose[62] spin systems. The peak multiplicities indicate the complex sugar linkages, hydrogen bonding patterns, and conformations of these polysaccharides. Only some of these ^{13}C chemical shifts had been reported in the literature, mostly based on studies of extracted polysaccharides.[17,50,53,63−65] Our connectivity-based *de novo* assignments are consistent with peak intensities, with carbons in the same monosaccharide unit showing similar intensities and line widths. The unique chemical shifts of Xn (102 ppm) and FA (56 ppm) are particularly useful for the assignment of GAX peaks.

The assigned ^{13}C chemical shifts allow us to detect, for the first time, intermolecular cross peaks between cellulose and GAX in the grass PCW (Figures 8 and 9). The cellulose cross peaks to FA and Ara are of particular interest, because they indicate that substituted GAX can approach the cellulose microfibrils on the ∼1 nm scale, which is the approximate distance upper limit of ^{13}C spin diffusion. This result counters the notion that highly substituted GAX cannot bind cellulose.[9] The quantitative 1D ^{13}C spectra (Figure 2) indicate an Ara/Xn intensity ratio of ∼0.78. This means that approximately three of four Xyl units are decorated with Ara, if we make the approximation that all arabinoses are located in GAX. Although some Ara exists in pectins and AGPs, these two polymers have very low concentrations in the wall; thus, the degree of GAX substitution should not be much lower than the estimate given

dx.doi.org/10.1021/bi500231b | *Biochemistry* 2014, 53, 2840−2854

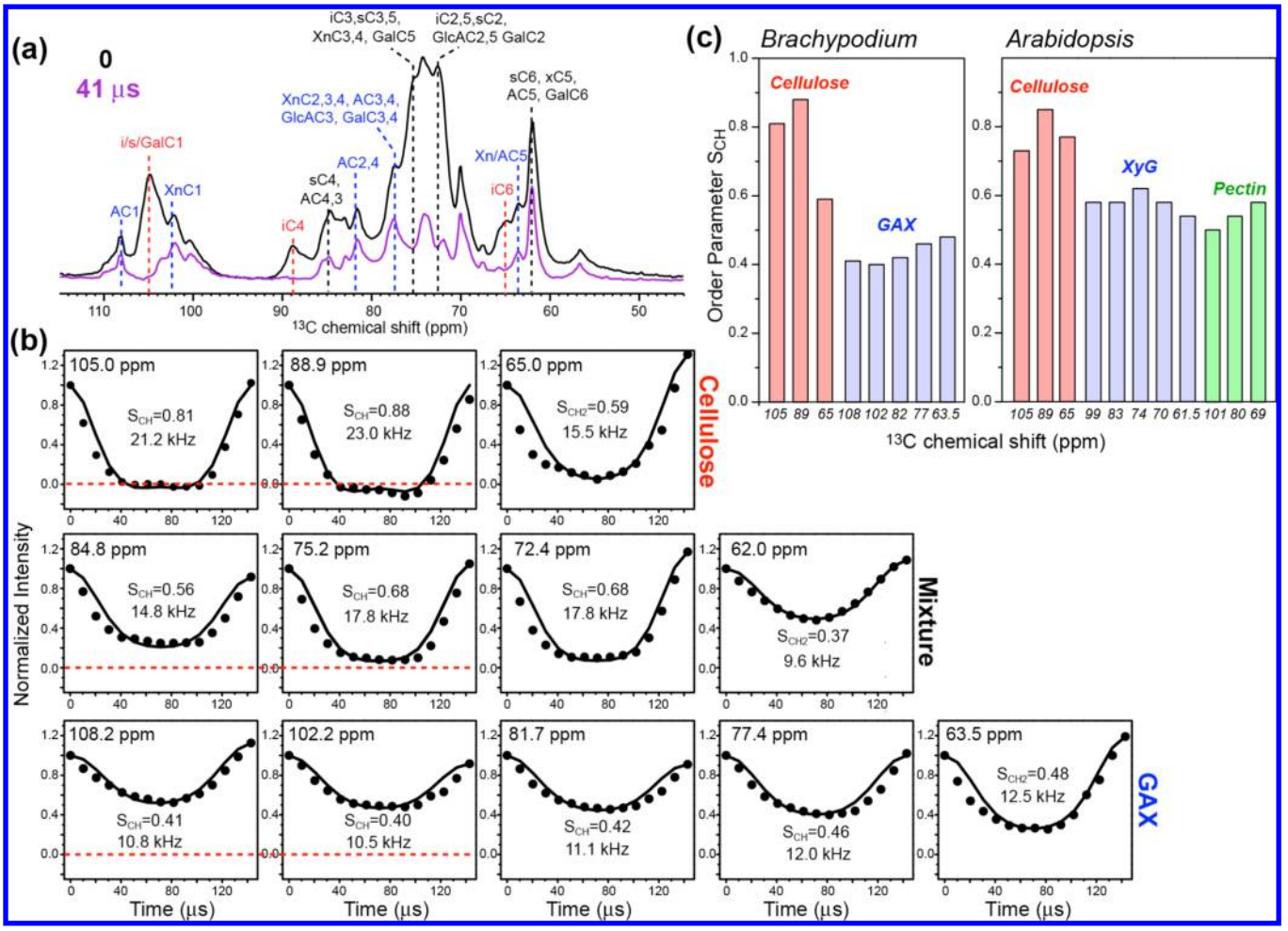

Figure 10. C−H order parameters of the *Brachypodium* wall polysaccharides compared with the *Arabidopsis* data at 293 K. (a) ω_2 cross sections of the *Brachypodium* 2D DIPSHIFT spectra with 0 and 41 μs dipolar dephasing. The cellulose peaks are mostly suppressed at 41 μs, while the GAX signals remain, indicating GAX is more dynamic. (b) ^{13}C−^{1}H dipolar dephasing curves of cellulose (top), GAX (bottom), and mixture peaks (middle) in the *Brachypodium* PCW. Dashed lines guide the eye for intensity comparisons. (c) C−H order parameters of *Brachypodium* (left) and *Arabidopsis* (right) PCWs. The order parameters of GAX are lower than those of XyG.

above. Therefore, the 2D ^{13}C spin diffusion spectra indicate that ~75% substituted GAX has molecular contact with cellulose. This result to some extent is not surprising, because in the absence of MLG, GAX is the dominant polysaccharide to cross-link cellulose, but because highly branched xylan chains cannot easily stack onto the cellulose surfaces, these intermolecular cross peaks imply that GAX surrounds the cellulose microfibrils in a disordered fashion. Moreover, the cellulose-interacting GAX domain must be a small fraction of all GAX, because the cellulose−GAX cross peaks are much weaker than the GAX−GAX and cellulose−cellulose cross peaks, and even with a mixing time of 1.5 s, the cellulose and GAX cross sections are far from equilibrated in their intensities (Figure 8). The fraction of GAX that is in molecular contact with cellulose can be estimated from the biexponential relaxation data, which show that ~60% of GAX has very short ^{13}C T_1 and ^{1}H $T_{1\rho}$ relaxation times (Figure 11). This means that the rigid GAX domain, which may be responsible for cross-linking cellulose, accounts for up to 40% of all GAX.

The *Brachypodium* PCW sample is more dynamic than the *Arabidopsis* sample, as manifested qualitatively by the many sharp signals in the 2D J-INADEQUATE spectrum, and quantitatively by the smaller C−H order parameters (~0.4) and shorter relaxation times of GAX compared to those of XyG in the *Arabidopsis* PCW. GAX shows large amplitude motions on both the nanosecond (^{13}C T_1) and microsecond (^{1}H $T_{1\rho}$) time scales, similar to XyG, but the fractions of the mobile component in GAX are larger than the mobile fractions of XyG in *Arabidopsis*. Compared to cellulose, the rigid GAX domain, which potentially interacts with cellulose, is still more mobile, as seen by its shorter relaxation times. This mobility difference is not inherently contradictory, because substantial dynamic gradients can occur within several bonds, as shown by ^{13}C-resolved ^{1}H line shapes of synthetic polymers[66] and proteins.[29,67] Overall, the main hemicellulose in the *Brachypodium* PCW has more heterogeneous dynamics than the main hemicellulose, GAX, in the *Arabidopsis* PCW.

Cellulose is rigid in both *Brachypodium* and *Arabidopsis* cell walls, with high order parameters of 0.7−0.9 for non-C6 groups, but the cellulose rigidity is not identical. The *Brachypodium* sample has a smaller C6 order parameter but longer ^{13}C T_1 and ^{1}H $T_{1\rho}$ relaxation times than the *Arabidopsis* sample. The former likely results from the influence of the highly dynamic GAX, which may promote larger amplitude motion of the protruding hydroxymethyl group. The latter observation, which implies faster motions of the *Arabidopsis*

dx.doi.org/10.1021/bi500231b | *Biochemistry* 2014, 53, 2840−2854

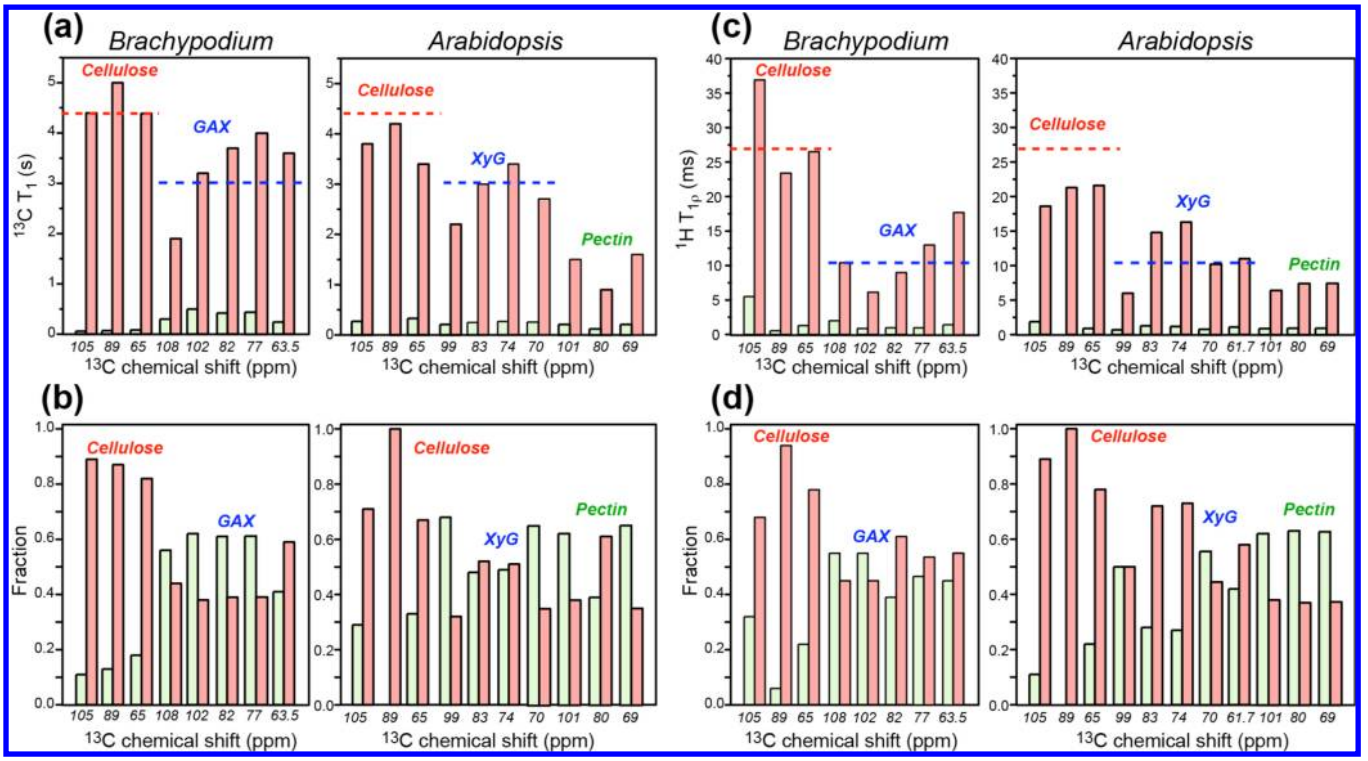

Figure 11. Relaxation times of grass and dicot wall polysaccharides. (a) ^{13}C T_1 relaxation times of *Brachypodium* (left) and *Arabidopsis* (right) PCWs. The long and short T_1 components are indicated in red and green, respectively. (b) Fractions of the two T_1 components. The polysaccharide signals are categorized as cellulose, hemicellulose, and pectin peaks. Dashed lines guide the eyes for the differences between the two CWs. (c) Site-specific ^{1}H $T_{1\rho}$ relaxation times. (d) Fractions of the two $T_{1\rho}$ components.

cellulose, is not fully understood. In general, the nanosecond motions that induce T_1 relaxation are fast torsional fluctuations, while the microsecond motions that induce $T_{1\rho}$ relaxation are likely collective motions of several sugar units. We hypothesize that the slightly faster motions of the dicot cellulose may be caused by the highly dynamic pectins, which are now known to interact with cellulose.[6,22]

In conclusion, this study provides the first comprehensive set of ^{13}C chemical shifts of the polysaccharides in the near-native *Brachypodium* PCW. At 2 weeks of age, the cell wall contains cellulose and GAX as the major polysaccharides, while pectins, XyG, and structural proteins are present at concentrations much lower than those in the *Arabidopsis* PCW at the same developmental stage. The GAX in the grass PCW is ∼75% substituted, and a small portion of this highly branched GAX contacts cellulose on the nanometer scale based on 2D correlation spectra. Bond order parameters and relaxation times indicate that GAX is heterogeneously dynamic: a dominant dynamic domain, which may fill the interfibrillar space, coexists with a minor rigid domain, which may be responsible for cross-linking the cellulose microfibrils. Thus, in the grass PCW, GAX takes on the dual structural and dynamical characteristics of XyG and pectins in the dicot PCW. A large number of arabinose structures and linkage patterns are observed, indicating that this monosaccharide acts as a versatile building block in the grass PCW.

■ ASSOCIATED CONTENT

Supporting Information

Additional NMR spectra and tables. This material is available free of charge via the Internet at http://pubs.acs.org.

■ AUTHOR INFORMATION

Corresponding Author

*E-mail: mhong@iastate.edu. Telephone: (515) 294-3521. Fax: (515) 294-0105.

Funding

This work was supported by the U.S. Department of Energy (DOE), Office of Basic Energy Sciences, Division of Materials Sciences and Engineering, under Contract DE-AC02-07CH11358 (to M.H.) and by National Science Foundation Grant 1121163 (to O.A.Z.). Linkage composition was performed at CCRC Analytical services supported by the DOE-funded Center for Plant and Microbial Complex Carbohydrates under Contract DE-FG02-93ER-20097.

Notes

The authors declare no competing financial interest.

■ ABBREVIATIONS

AGP, arabinogalactan protein; Ara or A, arabinan; FA, ferulic acid; GalA, galacturonic acid; G, glucose in xyloglucan; GlcA, glucuronic acid; GAX, glucuronoarabinoxylan; HGA, homogalacturonan; i, interior crystalline cellulose; MLG, mixed linkage glucan; s, surface amorphous cellulose; Rha or R, rhamnose; XyG, xyloglucan; Xyl, xylose; x, xylose in xyloglucan; Xn, xylose in glucuronoarabinoxylan; CP, cross-polarization; DP, direct polarization; MAS, magic-angle spinning; PCW, primary cell wall.

■ REFERENCES

(1) Ragauskas, A. J., Williams, C. K., Davison, B. H., Britovsek, G., Cairney, J., Eckert, C. A., Frederick, W. J., Hallett, J. P., Leak, D. J., Liotta, C. L., Mielenz, J. R., Murphy, R., Templer, R., and Tschaplinski,

T. (2006) The path forward for biofuels and biomaterials. *Science 311*, 484−489.
(2) Service, R. F. (2007) Cellulosic ethanol: Biofuel researchers prepare to reap a new harvest. *Science 315*, 1488−1491.
(3) McCann, M. C., and Carpita, N. C. (2008) Designing the deconstruction of plant cell walls. *Curr. Opin. Plant Biol. 11*, 314−320.
(4) Initiative, I. B. (2010) Genome sequencing and analysis of the model grass *Brachypodium distachyon*. *Nature 463*, 763−768.
(5) Carpita, N. C., and Gibeaut, D. M. (1993) Structural models of primary cell walls in flowering plants: Consistency of molecular structure with the physical properties of the walls during growth. *Plant J. 3*, 1−30.
(6) Dick-Perez, M., Zhang, Y., Hayes, J., Salazar, A., Zabotina, O. A., and Hong, M. (2011) Structure and interactions of plant cell-wall polysaccharides by two- and three-dimensional magic-angle-spinning solid-state NMR. *Biochemistry 50*, 989−1000.
(7) Buanafina, M. M. D. (2009) Feruloylation in Grasses: Current and Future Perspectives. *Mol. Plant 2*, 861−872.
(8) Carpita, N. C. (1984) Cell-Wall Development in Maize Coleoptiles. *Plant Physiol. 76*, 205−212.
(9) Carpita, N. C. (1996) Structure and biogenesis of the cell walls of grasses. *Annu. Rev. Plant Physiol. Plant Mol. Biol. 47*, 445−476.
(10) Vogel, J. (2008) Unique aspects of the grass cell wall. *Curr. Opin. Plant Biol. 11*, 301−307.
(11) Nishiyama, Y., Langan, P., and Chanzy, H. (2002) Crystal structure and hydrogen-bonding system in cellulose 1β from synchrotron X-ray and neutron fiber diffraction. *J. Am. Chem. Soc. 124*, 9074−9082.
(12) Nishiyama, Y., Sugiyama, J., Chanzy, H., and Langan, P. (2003) Crystal structure and hydrogen bonding system in cellulose 1α, from synchrotron X-ray and neutron fiber diffraction. *J. Am. Chem. Soc. 125*, 14300−14306.
(13) Ding, S. Y., Liu, Y. S., Zeng, Y. N., Himmel, M. E., Baker, J. O., and Bayer, E. A. (2012) How Does Plant Cell Wall Nanoscale Architecture Correlate with Enzymatic Digestibility? *Science 338*, 1055−1060.
(14) Marga, F., Grandbois, M., Cosgrove, D. J., and Baskin, T. I. (2005) Cell wall extension results in the coordinate separation of parallel microfibrils: Evidence from scanning electron microscopy and atomic force microscopy. *Plant J. 43*, 181−190.
(15) Zhang, T., Mahgsoudy-Louyeh, S., Tittmann, B., and Cosgrove, D. (2013) Visualization of the nanoscale pattern of recently-deposited cellulose microfibrils and matrix materials in never-dried primary walls of the onion epidermis. *Cellulose*, 1−10.
(16) Lu, F., and Ralph, J. (2003) Non-degradative dissolution and acetylation of ball-milled plant cell walls: High-resolution solution-state NMR. *Plant J. 35*, 535−544.
(17) Cheng, K., Sorek, H., Zimmermann, H., Wemmer, D. E., and Pauly, M. (2013) Solution-state 2D NMR spectroscopy of plant cell walls enabled by a dimethylsulfoxide-d6/1-ethyl-3-methylimidazolium acetate solvent. *Anal. Chem. 85*, 3213−3221.
(18) Atalla, R. H., and VanderHart, D. L. (1984) Native Cellulose: A Composite of Two Distinct Crystalline Forms. *Science 223*, 283−285.
(19) Vietor, R. J., Newman, R. H., Ha, M. A., Apperley, D. C., and Jarvis, M. C. (2002) Conformational features of crystal-surface cellulose from higher plants. *Plant J. 30*, 721−731.
(20) Jarvis, M. (2003) Chemistry: Cellulose stacks up. *Nature 426*, 611−612.
(21) Dick-Perez, M., Wang, T., Salazar, A., Zabotina, O. A., and Hong, M. (2012) Multidimensional solid-state NMR studies of the structure and dynamics of pectic polysaccharides in uniformly ^{13}C-labeled *Arabidopsis* primary cell walls. *Magn. Reson. Chem. 50*, 539−550.
(22) Wang, T., Zabotina, O., and Hong, M. (2012) Pectin-cellulose interactions in the *Arabidopsis* primary cell wall from two-dimensional magic-angle-spinning solid-state nuclear magnetic resonance. *Biochemistry 51*, 9846−9856.
(23) Wang, T., Park, Y. B., Caporini, M. A., Rosay, M., Zhong, L., Cosgrove, D. J., and Hong, M. (2013) Sensitivity-enhanced solid-state NMR detection of expansin's target in plant cell walls. *Proc. Natl. Acad. Sci. U.S.A. 110*, 16444−16449.
(24) Sloneker, J. H. (1971) Determination of cellulose and apparent hemicellulose in plant tissue by gas-liquid chromatography. *Anal. Biochem. 43*, 539−546.
(25) Carpita, N. C. (1983) Hemicellulosic Polymers of Cell-Walls of Zea Coleoptiles. *Plant Physiol. 72*, 515−521.
(26) Carpita, N. C., Defernez, M., Findlay, K., Wells, B., Shoue, D. A., Catchpole, G., Wilson, R. H., and McCann, M. C. (2001) Cell wall architecture of the elongating maize coleoptile. *Plant Physiol. 127*, 551−565.
(27) Whitney, S. E., Gothard, M. G., Mitchell, J. T., and Gidley, M. J. (1999) Roles of cellulose and xyloglucan in determining the mechanical properties of primary plant cell walls. *Plant Physiol. 121*, 657−664.
(28) Whitney, S. E. C., Brigham, J. E., Darke, A. H., Reid, J. S. G., and Gidley, M. J. (1995) In-Vitro Assembly of Cellulose/Xyloglucan Networks: Ultrastructural and Molecular Aspects. *Plant J. 8*, 491−504.
(29) Hong, M., and Griffin, R. G. (1998) Resonance Assignment for Solid Peptides by Dipolar-Mediated ^{13}C/^{15}N Correlation Solid-State NMR. *J. Am. Chem. Soc. 120*, 7113−7114.
(30) Rienstra, C. M., Hohwy, M., Hong, M., and Griffin, R. G. (2000) 2D and 3D ^{15}N-^{13}C-^{13}C NMR chemical shift correlation spectroscopy of solids: Assignment of MAS spectra of peptides. *J. Am. Chem. Soc. 122*, 10979−10990.
(31) Bax, A., Freeman, R., and Kempsell, S. P. (1980) Natural-abundance ^{13}C-^{13}C coupling observed via double-quantum coherence. *J. Am. Chem. Soc. 102*, 4849−4851.
(32) Lesage, A., Auger, C., Caldarelli, S., and Emsley, L. (1997) Determination of through-bond carbon-carbon connectivities in solid-state NMR using the INADEQUATE experiment. *J. Am. Chem. Soc. 119*, 7867−7868.
(33) Hohwy, M., Jakobsen, H. J., Eden, M., Levitt, M. H., and Nielsen, N. C. (1998) Broadband dipolar recoupling in the nuclear magnetic resonance of rotating solids: A compensated C7 pulse sequence. *J. Chem. Phys. 108*, 2686−2694.
(34) Takegoshi, K., Nakamura, S., and Terao, T. (2001) C-13-H-1 dipolar-assisted rotational resonance in magic-angle spinning NMR. *Chem. Phys. Lett. 344*, 631−637.
(35) Munowitz, M. G., Griffin, R. G., Bodenhausen, G., and Huang, T. H. (1981) Two-dimensional rotational spin-echo NMR in solids: Correlation of chemical shift and dipolar interactions. *J. Am. Chem. Soc. 103*, 2529−2533.
(36) Hong, M., Gross, J. D., Rienstra, C. M., Griffin, R. G., Kumashiro, K. K., and Schmidt-Rohr, K. (1997) Coupling Amplification in 2D MAS NMR and Its Application to Torsion Angle Determination in Peptides. *J. Magn. Reson. 129*, 85−92.
(37) Bielecki, A., Kolbert, A. C., and Levitt, M. H. (1989) Frequency-switched pulse sequences: Homonuclear decoupling and dilute spin NMR in solids. *Chem. Phys. Lett. 155*, 341−346.
(38) Rienstra, C. M., Tucker-Kellogg, L., Jaroniec, C. P., Hohwy, M., Reif, B., McMahon, M. T., Tidor, B., Lozano-Perez, T., and Griffin, R. G. (2002) De novo determination of peptide structure with solid-state magic-angle spinning NMR spectroscopy. *Proc. Natl. Acad. Sci. U.S.A. 99*, 10260−10265.
(39) Hong, M., Yao, X. L., Jakes, K., and Huster, D. (2002) Investigation of molecular motions by Lee-Goldburg cross-polarization NMR spectroscopy. *J. Phys. Chem. B 106*, 7355−7364.
(40) Huster, D., Xiao, L., and Hong, M. (2001) Solid-state NMR investigation of the dynamics of the soluble and membrane-bound colicin Ia channel-forming domain. *Biochemistry 40*, 7662−7674.
(41) van Rossum, B. J., de Groot, C. P., Ladizhansky, V., Vega, S., and de Groot, H. J. M. (2000) A method for measuring heteronuclear (H-1-C-13) distances in high speed MAS NMR. *J. Am. Chem. Soc. 122*, 3465−3472.
(42) York, W. S., Darvill, A. G., McNeil, M., Stevenson, T. T., and Albersheim, P. (1985) Isolation and characterization of plant cell walls and cell-wall components. *Methods Enzymol. 118*, 3−40.

(43) Ciucanu, I., and Kerek, F. (1984) A simple and rapid method for the permethylation of carbohydrates. *Carbohydr. Res. 131*, 209−217.
(44) Seifert, G. J., and Roberts, K. (2007) The biology of arabinogalactan proteins. *Annu. Rev. Plant Biol. 58*, 137−161.
(45) Fincher, G. B., Stone, B. A., and Clarke, A. E. (1983) Arabinogalactan-Proteins: Structure, Biosynthesis, and Function. *Annu. Rev. Plant Physiol. Plant Mol. Biol. 34*, 47−70.
(46) Showalter, A. M. (1993) Structure and Function of Plant-Cell Wall Proteins. *Plant Cell 5*, 9−23.
(47) Buckeridge, M. S., Rayon, C., Urbanowicz, B., Tine, M. A. S., and Carpita, N. C. (2004) Mixed linkage (1 → 3),(1 → 4)-β-D-glucans of grasses. *Cereal Chem. 81*, 115−127.
(48) Burton, R. A., and Fincher, G. B. (2009) (1,3;1,4)-β-D-Glucans in cell walls of the poaceae, lower plants, and fungi: A tale of two linkages. *Mol. Plant 2*, 873−882.
(49) Hong, M. (1999) Solid-state dipolar INADEQUATE NMR spectroscopy with a large double-quantum spectral width. *J. Magn. Reson. 136*, 86−91.
(50) Hollmann, J., Elbegzaya, N., Pawelzik, E., and Lindhauer, M. G. (2009) Isolation and characterization of glucuronoarabinoxylans from wheat bran obtained by classical and ultrasound-assisted extraction methods. *Qual. Assur. Saf. Crops Foods 1*, 231−239.
(51) Roubroeks, J. P., Andersson, R., and Aman, P. (2000) Structural features of (1 → 3),(1 → 4)-β-D-glucan and arabinoxylan fractions isolated from rye bran. *Carbohydr. Polym. 42*, 3−11.
(52) Tan, L., Varnai, P., Lamport, D. T., Yuan, C., Xu, J., Qiu, F., and Kieliszewski, M. J. (2010) Plant O-hydroxyproline arabinogalactans are composed of repeating trigalactosyl subunits with short bifurcated side chains. *J. Biol. Chem. 285*, 24575−24583.
(53) Habibi, Y., Mahrouz, M., and Vignon, M. R. (2005) Arabinan-rich polysaccharides isolated and characterized from the endosperm of the seed of Opuntia ficus-indica prickly pear fruits. *Carbohydr. Polym. 60*, 319−329.
(54) Buchanan, B. B., Gruissem, W., and Jones, R. L. (2000) *Biochemistry and Molecular Biology of Plants*, American Society of Plant Physiologists, Rockville, MD.
(55) Kabel, M. A., de Waard, P., Schols, H. A., and Voragen, A. G. (2003) Location of O-acetyl substituents in xylo-oligosaccharides obtained from hydrothermally treated Eucalyptus wood. *Carbohydr. Res. 338*, 69−77.
(56) Gille, S., and Pauly, M. (2012) O-acetylation of plant cell wall polysaccharides. *Front. Plant Sci. 3*, 12.
(57) Roubroeks, J. P., Andersson, R., Mastromauro, D. I., Christensen, B. E., and Aman, P. (2001) Molecular weight, structure and shape of oat (1 → 3),(1 → 4)-β-D-glucan fractions obtained by enzymatic degradation with (1 → 4)-β-D-glucan 4-glucanohydrolase from *Trichoderma reesei*. *Carbohydr. Polym. 46*, 275−285.
(58) Bowles, R. K., Morgan, K. R., Furneaux, R. H., and Coles, G. D. (1996) C-13 CP/MAS NMR study of the interaction of bile acids with barley β-D-glucan. *Carbohydr. Polym. 29*, 7−10.
(59) Wood, P. J., Weisz, J., and Blackwell, B. A. (1994) Structural Studies of (1→3),(1→4)-β-D-Glucans by ^{13}C-Nuclear Magnetic-Resonance Spectroscopy and by Rapid Analysis of Cellulose-Like Regions Using High-Performance Anion-Exchange Chromatography of Oligosaccharides Released by Lichenase. *Cereal Chem. 71*, 301−307.
(60) Rancour, D. M., Marita, J. M., and Hatfield, R. D. (2012) Cell wall composition throughout development for the model grass *Brachypodium distachyon*. *Front. Plant Sci. 3*, 266.
(61) Christensen, U., Alonso-Simon, A., Scheller, H. V., Willats, W. G. T., and Harholt, J. (2010) Characterization of the primary cell wlls of seedlings of *Brachypodium distachyon*: A potential model plant for temperate grasses. *Phytochemistry 71*, 62−69.
(62) Harris, D. M., Corbin, K., Wang, T., Gutierrez, R., Bertolo, A. L., Petti, C., Smilgies, D. M., Estevez, J. M., Bonetta, D., Urbanowicz, B. R., Ehrhardt, D. W., Somerville, C. R., Rose, J. K., Hong, M., and Debolt, S. (2012) Cellulose microfibril crystallinity is reduced by mutating C-terminal transmembrane region residues CESA1A903V and CESA3T942I of cellulose synthase. *Proc. Natl. Acad. Sci. U.S.A. 109*, 4098−4103.
(63) Dourado, F., Cardoso, S. M., Silva, A. M. S., Gama, F. M., and Coimbra, M. A. (2006) NMR structural elucidation of the arabinan from *Prunus dulcis* immunobiological active pectic polysaccharides. *Carbohydr. Polym. 66*, 27−33.
(64) Vignon, M. R., and Gey, C. (1998) Isolation, H-1 and C-13 NMR studies of (4-O-methyl-D-glucurono)-D-xylans from luffa fruit fibres, jute bast fibres and mucilage of quince tree seeds. *Carbohydr. Res. 307*, 107−111.
(65) Bunzel, M., Ralph, J., Funk, C., and Steinhart, H. (2005) Structural elucidation of new ferulic acid-containing phenolic dimers and trimers isolated from maize bran. *Tetrahedron Lett. 46*, 5845−5850.
(66) Schmidt-Rohr, K., and Spiess, H. W. (1994) *Multidimensional Solid-State NMR and Polymers*, Academic Press, San Diego.
(67) Park, Y. B., and Cosgrove, D. J. (2012) A revised architecture of primary cell walls based on biomechanical changes induced by substrate-specific endoglucanases. *Plant Physiol. 158*, 1933−1943.
(68) Hromadkova, Z., Ebringerova, A., and Valachovic, P. (2002) Ultrasound-assisted extraction of water-soluble polysaccharides from the roots of valerian (*Valeriana officinalis* L.). *Ultrason. Sonochem. 9*, 37−44.
(69) Jarvis, M. C. (1990) The C-13-Nmr Spectrum of (1→4)-β-Deuterium-Mannans in Intact Endosperm Tissue of the Date (*Phoenix dactylifera*). *Carbohydr. Res. 197*, 276−280.

Supporting Information

Structure and Dynamics of *Brachypodium* Primary Cell Wall Polysaccharides from Two-Dimensional ^{13}C Solid-State Nuclear Magnetic Resonance Spectroscopy

Tuo Wang [1], Andre Salazar [2], Olga A. Zabotina[2], and Mei Hong[1]

[1]Department of Chemistry and the Ames Laboratory, [2]Department of Biochemistry, Biophysics & Molecular Biology, Iowa State University, Ames, IA 50011

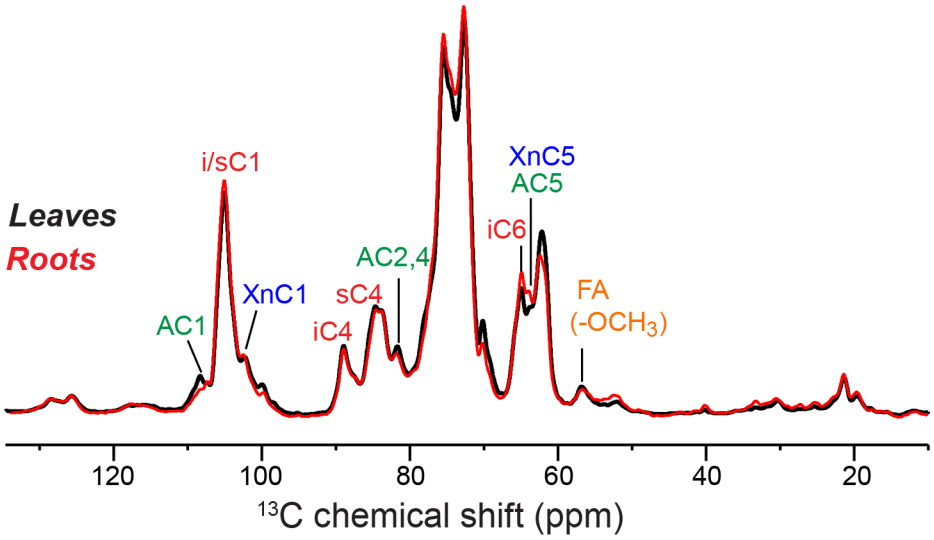

Figure S1. 1D ^{13}C CP-MAS spectrum of *Brachypodium* primary cell walls from leaves (black) and roots (red). The spectra were measured at 293 K under 8 kHz MAS, and were processed using Gaussian multiplication parameters of LB=-70, and GB = 0.5.

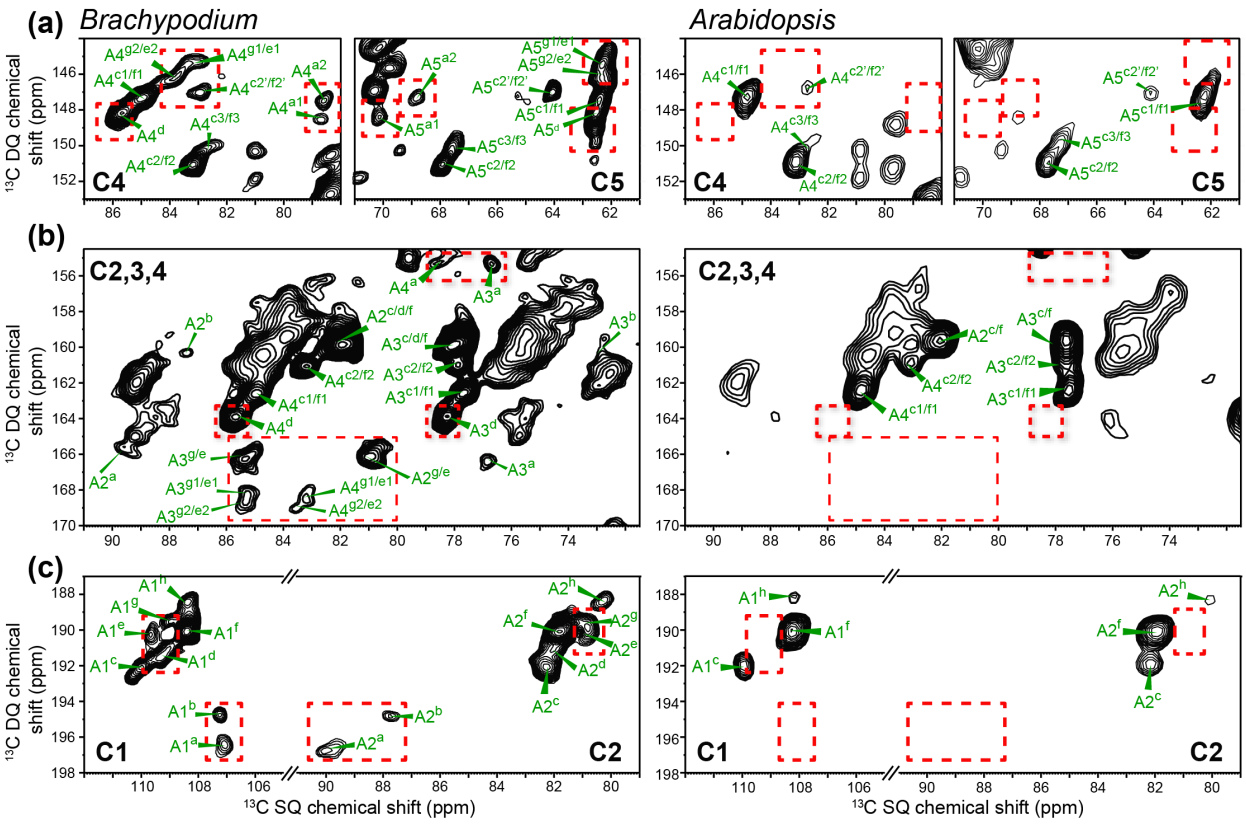

Figure S2. Comparison of the Ara signals between *Brachypodium* (left) and *Arabidopsis* (right) PCWs from 2D ^{13}C J-INADEQUATE spectra. New Ara signals in the *Brachypodium* PCW are highlighted with dashed boxes. (a) C4-C5 correlations. (b) C2-C3-C4 correlations. (c) C1-C2 correlations.

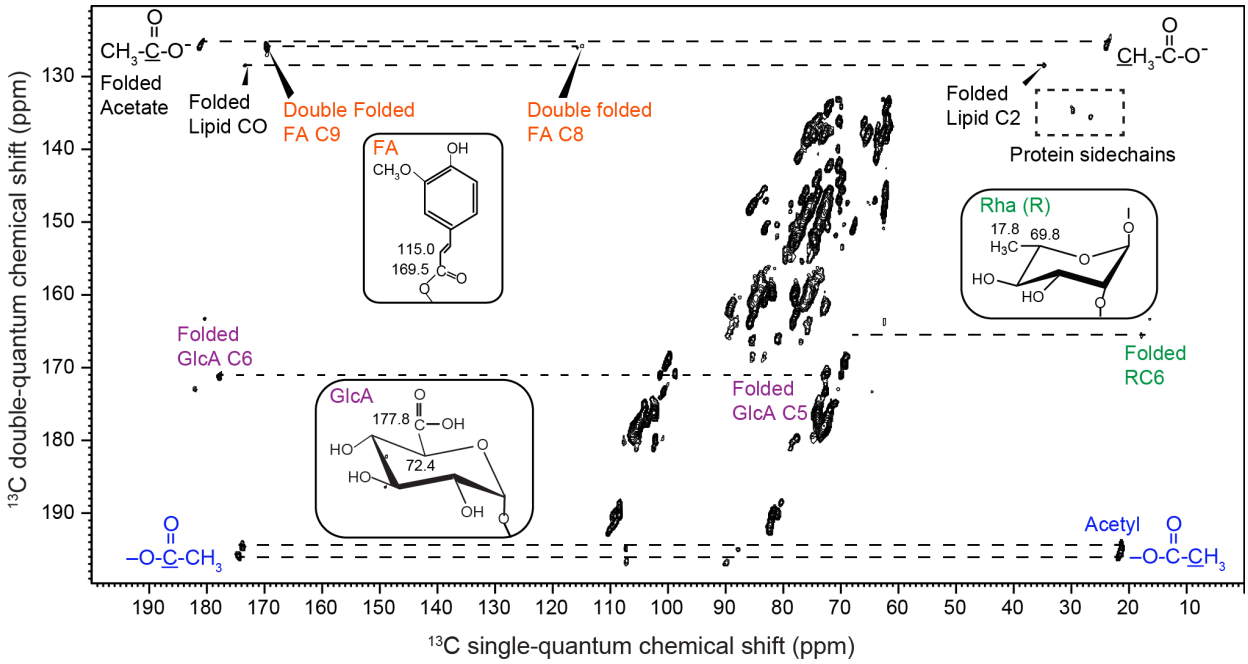

Figure S3. Full 2D ^{13}C J-INADEQUATE spectrum of *Brachypodium* PCW. The ω_1 spectral width is 79.5 ppm, thus some cross peaks were folded. A few weak protein signals are seen (dashed box). No protein-polysaccharide cross peaks are detected. Clear cross peaks of acetyl groups, GlcA C5-C6, FA C8-C9 and Rha C5-C6 are resolved, and indicate the dynamic nature of these groups. The acetate cross peaks at (181, 24) ppm result from the sodium acetate used in the CW preparation.

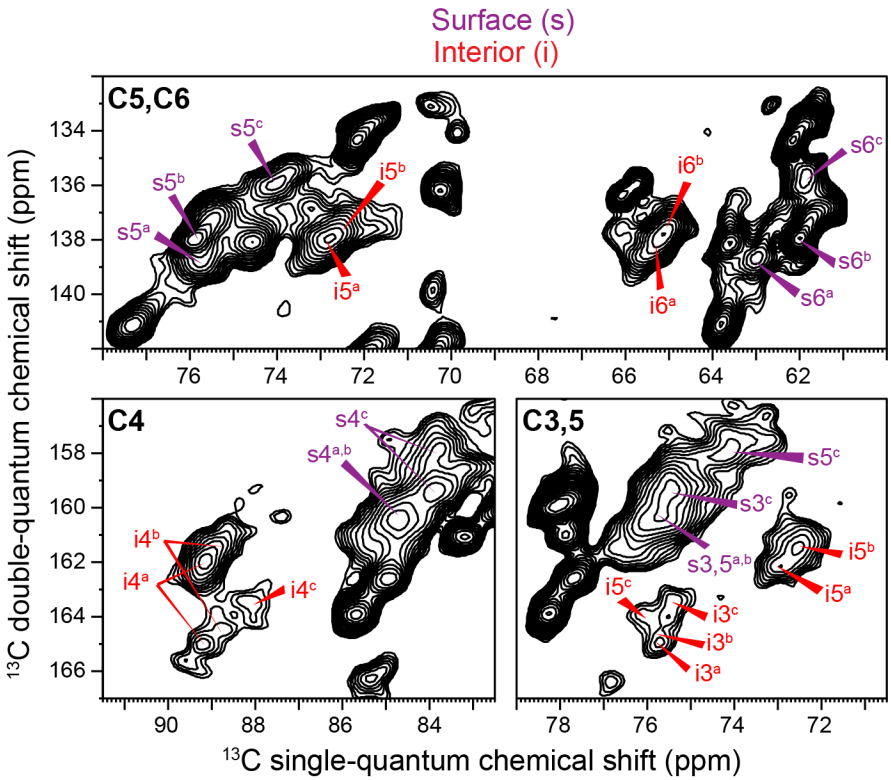

Figure S4. Interior crystalline and surface amorphous cellulose signals from the 2D ^{13}C J-INADEQUATE spectrum of *Brachypodium* PCW. At least three sets each of the cellulose signals are resolved, as denoted by superscripts a, b, c.

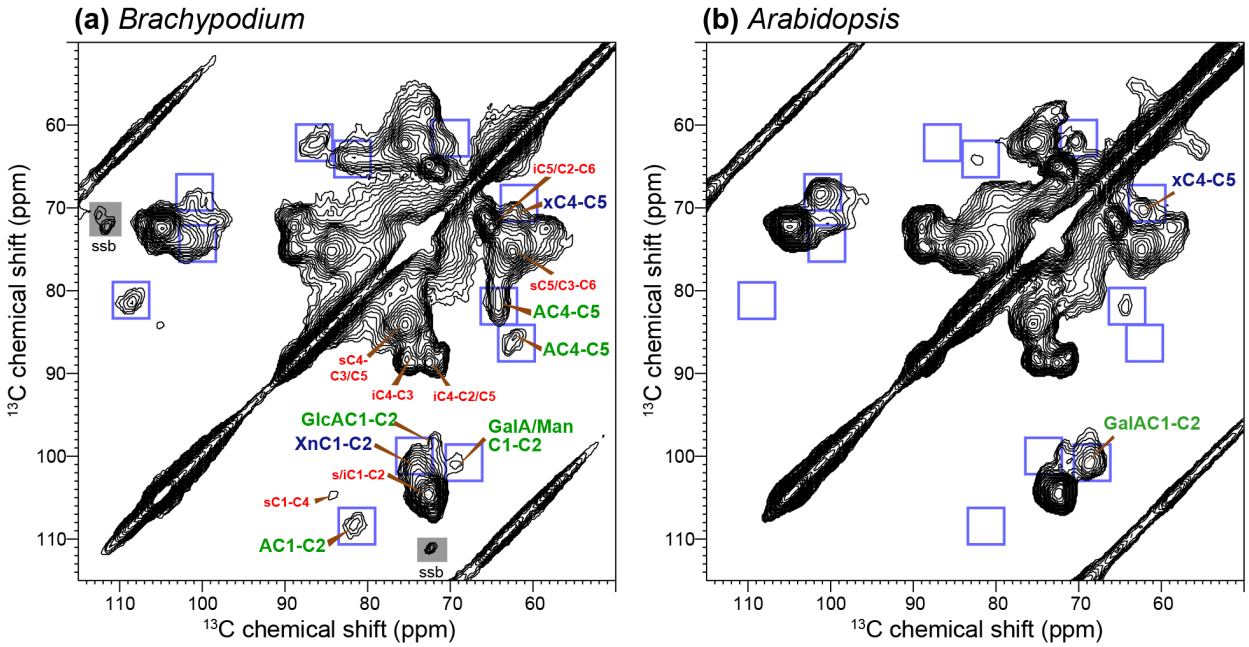

Figure S5. 2D DQF ^{13}C correlation spectra of (a) *Brachypodium* and (b) *Arabidopsis* PCWs. *Brachypodium* shows more Xn, Ara and GlcA signals and less GalA and XyG signals than *Arabidopsis*. The spectra were measured at 253 K under 7 kHz MAS.

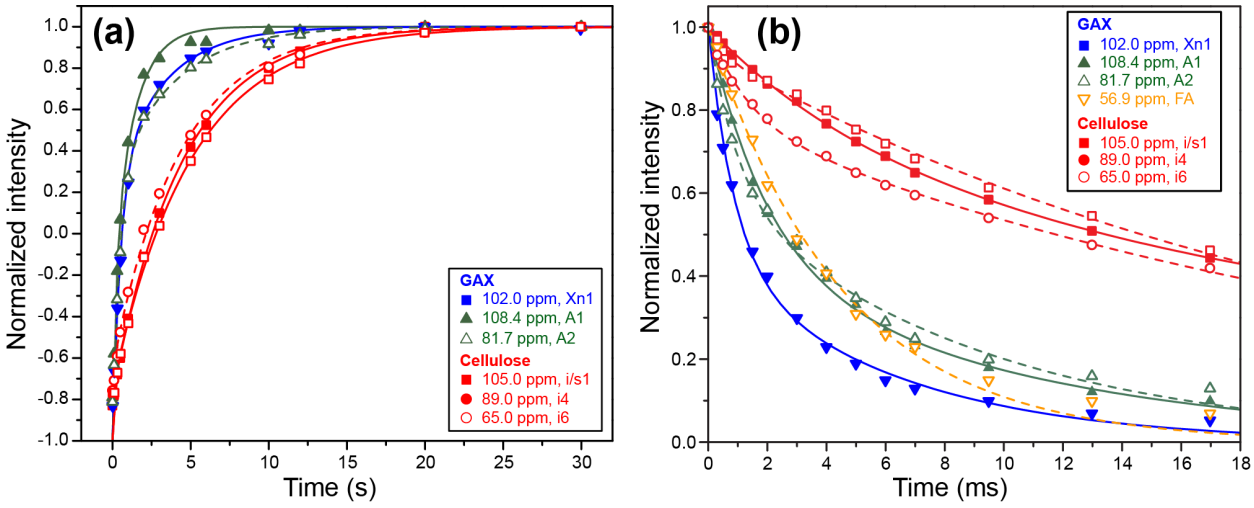

Figure S6. Representative relaxation data of *Brachypodium* wall polysaccharides. (a) Quantitative ^{13}C T_1 inversion recovery curves measured with a 15 s recycle delay. (b) ^{1}H $T_{1\rho}$ relaxation curves measured using a Lee-Goldburg spin-lock sequence. Cellulose, xylan, arabinose and ferulic acid signals are shown in red, blue, green and yellow, respectively. GAX displays much shorter ^{13}C T_1's and ^{1}H $T_{1\rho}$ values than cellulose.

Table S1. Quantitative ^{13}C T_1 relaxation times (s) of *Brachypodium* PCW polysaccharides. The double exponential fitting function is $I(t) = a\left(1 - 2e^{-t/T_{1a}}\right) + b\left(1 - 2e^{-t/T_{1b}}\right)$, where b = 1-a.

Assignment	δ_C (ppm)	a (mobile)	b (rigid)	T_{1a} (s)	T_{1b} (s)
AC1	108.4	0.41±0.17	0.59±0.17	0.22±0.11	1.4±0.4
AC1	108.0	0.56±0.15	0.44±0.15	0.30±0.10	1.9±0.6
i/sC1	105.0	0.11±0.02	0.89±0.02	0.06±0.06	4.4±0.2
XnC1	102.0	0.62±0.12	0.38±0.12	0.50±0.11	3.2±1.0
iC4	89.0	0.13±0.03	0.87±0.03	0.07±0.07	5.0±0.4
sC4, AC3,4	84.8	0.40±0.06	0.60±0.06	0.31±0.09	4.3±0.6
AC2	81.7	0.61±0.09	0.39±0.09	0.42±0.09	3.7±1.0
XnC2,3,4, AC3,4, GlcAC3, GalC5	77.4	0.61±0.08	0.39±0.08	0.44±0.08	4.0±0.9
iC3, sC3,5, XnC3,4, GalC5	75.4	0.24±0.05	0.76±0.05	0.23±0.11	4.2±0.4
iC2,5, sC2, GlcAC2,5, GalC2	72.7	0.21±0.04	0.79±0.04	0.19±0.10	4.3±0.4
iC6	65.0	0.18±0.04	0.82±0.04	0.09±0.07	4.4±0.4
A/XnC5	63.6	0.41±0.07	0.59±0.07	0.24±0.08	3.6±0.6
sC6, xC5, AC5, GalC6	62.0	0.58±0.05	0.42±0.05	0.22±0.04	3.2±0.6

Table S2. ^{1}H $T_{1\rho}$ relaxation times of *Brachypodium* cell wall polysaccharides. A double exponential function $I(t) = ae^{-t/T_{1\rho,a}} + be^{-t/T_{1\rho,b}}$ where b = 1-a was used to fit most of the data. A single exponential decay $I(t) = e^{-t/T_{1\rho}}$ was used to fit the data of FA (OMe).

Assignment	δ_C (ppm)	a (mobile)	b (rigid)	$T_{1\rho,a}$ (ms)	$T_{1\rho,b}$ (ms)
AC1	108.4	0.55±0.08	0.45±0.08	2.0±0.3	10±2
i/sC1	105.0	0.32±0.08	0.68±0.08	5.5±1.0	37±8
XnC1	102.0	0.55±0.05	0.45±0.05	0.9±0.1	6.2±0.8
iC4	89.0	0.06±0.01	0.94±0.01	0.6±0.2	23.4±0.6
sC4, AC3,4	84.8	0.24±0.03	0.76±0.03	1.7 ±0.3	22±2
AC2	81.7	0.39±0.05	0.61±0.05	1.0±0.2	9.0±0.9
XnC2,3,4, AC3,4, GlcAC3, GalC5	77.4	0.47±0.03	0.53±0.03	1.0±0.1	13±1
iC3, sC3,5, XnC3,4, GalC5	75.4	0.27±0.02	0.73±0.02	1.7±0.2	22±1
iC2,5, sC2, GlcAC2,5, GalC2	72.8	0.27±0.01	0.73±0.01	2.6±0.1	26±1
iC6	65.0	0.22±0.01	0.78±0.01	1.3±0.1	27±1
A/XnC5	63.6	0.45±0.02	0.55±0.02	1.5±0.1	18±2
sC6, xC5, AC5, GalC6	62.0	0.53±0.04	0.47±0.04	2.7±0.2	29±5
FA (OMe)	56.8		1		4.6±0.1